Effects of Strength and Stiffness Degradation on Seismic Response

FEMA P440A

June 2009

FEMA

nehrp

Effects of Strength and Stiffness Degradation on Seismic Response

Prepared by

APPLIED TECHNOLOGY COUNCIL
201 Redwood Shores Parkway, Suite 240
Redwood City, California 94065
www.ATCouncil.org

Prepared for

FEDERAL EMERGENCY MANAGEMENT AGENCY
Department of Homeland Security (DHS)

Michael Mahoney, Project Officer
Robert D. Hanson, Technical Monitor
Washington, D.C.

ATC MANAGEMENT AND OVERSIGHT
Christopher Rojahn (Project Executive)
Jon A. Heintz (Project Quality Control Monitor)
William T. Holmes (Project Tech. Monitor)

PROJECT MANAGEMENT COMMITTEE
Craig Comartin (Project Technical Director)
Eduardo Miranda
Michael Valley

PROJECT REVIEW PANEL
Kenneth Elwood
Subhash Goel
Farzad Naeim

CONSULTANT
Dimitrios Vamvatsikos

Notice

Foreword

One of the primary goals of the Federal Emergency Management Agency (FEMA) and the National Earthquake Hazards Reduction Program (NEHRP) is to encourage design and construction practices that address the earthquake hazard and minimize the potential damage resulting from that hazard. This document, *Effects of Strength and Stiffness on Degradation on Seismic Response* (FEMA P440A), is a follow-on publication to *Improvement of Nonlinear Static Seismic Analysis Procedures* (FEMA 440). It builds on another FEMA publication addressing the seismic retrofit of existing buildings, the *Prestandard and Commentary for Seismic Rehabilitation of Buildings* (FEMA 356) and the subsequent publication, ASCE/SEI Standard 41-06 *Seismic Rehabilitation of Existing Buildings* (ASCE 41).

The goal of FEMA 440 was improvement of nonlinear static analysis procedures, as depicted in FEMA 356 and ASCE 41, and development of guidance on when and how such procedures should be used. It was a resource guide for capturing the current state of the art in improved understanding of nonlinear static procedures, and for generating future improvements to those products. One of the recommendations to come out of that work was to fund additional studies of cyclic and in-cycle strength and stiffness degradation, and their impact on response and response stability.

This publication provides information that will improve nonlinear analysis for cyclic response, considering cyclic and in-cycle degradation of strength and stiffness. Recent work has demonstrated that it is important to be able to differentiate between cyclic and in-cycle degradation in order to more accurately model degrading behavior, while current practice only recognizes cyclic degradation, or does not distinguish between the two. The material contained within this publication is expected to improve nonlinear modeling of structural systems, and ultimately make the seismic retrofit of existing hazardous buildings more cost-effective.

This publication reaffirms FEMA's ongoing efforts to improve the seismic safety of new and existing buildings nationwide. This project is an excellent example of the interagency cooperation that is made possible through the NEHRP. FEMA is proud to have sponsored the development of this resource document through the Applied Technology Council (ATC), and is grateful

for work done by the Project Technical Director, Craig Comartin, the Project Management Committee, the Project Review Panel, the Project Working Group, and all other contributors who made this publication possible. All those who participated are listed at the end of this document, and FEMA appreciates their involvement.

Federal Emergency Management Agency

Preface

In September 2004 the Applied Technology Council (ATC) was awarded a "Seismic and Multi-Hazard Technical Guidance Development and Support" contract (HSFEHQ-04-D-0641) by the Federal Emergency Management Agency (FEMA) to conduct a variety of tasks, including one entitled "Advanced Seismic Analysis Methods – Resolution of Issues" (ATC-62 Project). The purpose of this project was to resolve a series of difficult technical issues that were identified during the preparation of the FEMA 440 report, *Improvement of Nonlinear Static Seismic Analysis Procedures* (FEMA, 2005).

FEMA 440 was funded by FEMA to develop improvements to nonlinear static analysis procedures contained in the FEMA 356 *Prestandard and Commentary for the Seismic Rehabilitation of Buildings* (FEMA, 2000), and the ATC-40 Report, *Seismic Evaluation and Retrofit of Concrete Buildings* (ATC, 1996). Unresolved technical issues identified in FEMA 440 included the need for additional guidance and direction on: (1) component and global modeling to consider nonlinear degrading response; (2) soil and foundation-structure interaction modeling; and (3) simplified nonlinear multiple-degree-of-freedom modeling.

Of these issues, this project has investigated nonlinear degrading response and conducted limited initial studies on multiple-degree-of-freedom effects. Work has included an extensive literature search and review of past studies on nonlinear strength and stiffness degradation, and review of available hysteretic models for capturing degrading strength and stiffness behavior. To supplement the existing body of knowledge, focused analytical studies were performed to explore the effects of nonlinear degradation on structural response. This report presents the findings and recommendations resulting from these efforts.

ATC is indebted to the members of the ATC-62 Project Team who participated in the preparation of this report. Direction of technical activities, review, and development of detailed recommendations were performed by the Project Management Committee, consisting of Craig Comartin (Project Technical Director), Eduardo Miranda, and Michael Valley. Literature reviews and focused analytical studies were conducted by Dimitrios Vamvatsikos. Technical review and comment at critical developmental

stages were provided by the Project Review Panel, consisting of Kenneth Elwood, Subhash Goel, and Farzad Naeim. A workshop of invited experts was convened to obtain feedback on preliminary findings and recommendations, and input from this group was instrumental in shaping the final product. The names and affiliations individuals who contributed to this work are included in the list of Project Participants provided at the end of this report.

ATC also gratefully acknowledges Michael Mahoney (FEMA Project Officer), Robert Hanson (FEMA Technical Monitor), and William Holmes (ATC Project Technical Monitor) for their input and guidance in the preparation of this report, Peter N. Mork for ATC report production services, and David Hutchinson as ATC Board Contact.

Jon A. Heintz
ATC Director of Projects

Christopher Rojahn
ATC Executive Director

Executive Summary

Much of the nation's work regarding performance-based seismic design has been funded by the Federal Emergency Management Agency (FEMA), under its role in the National Earthquake Hazards Reduction Program (NEHRP). Prevailing practice for performance-based seismic design is based on FEMA 273, *NEHRP Guidelines for the Seismic Rehabilitation of Buildings* (FEMA, 1997) and its successor documents, FEMA 356, *Prestandard and Commentary for the Seismic Rehabilitation of Buildings* (FEMA, 2000), and ASCE/SEI Standard 41-06, *Seismic Rehabilitation of Existing Buildings* (ASCE, 2006b). This series of documents has been under development for over twenty years, and has been increasingly absorbed into engineering practice over that period.

The FEMA 440 report, *Improvement of Nonlinear Static Seismic Analysis Procedures* (FEMA, 2005), was commissioned to evaluate and develop improvements to nonlinear static analysis procedures used in prevailing practice. Recommendations contained within FEMA 440 resulted in immediate improvement in nonlinear static analysis procedures, and were incorporated in the development of ASCE/SEI 41-06. However, several difficult technical issues remained unresolved.

1. Project Objectives

The Applied Technology Council (ATC) was commissioned by FEMA under the ATC-62 Project to further investigate the issue of component and global response to degradation of strength and stiffness. Using FEMA 440 as a starting point, the objectives of the project were to advance the understanding of degradation and dynamic instability by:

- Investigating and documenting currently available empirical and theoretical knowledge on nonlinear cyclic and in-cycle strength and stiffness degradation, and their affects on the stability of structural systems
- Supplementing and refining the existing knowledge base with focused analytical studies

- Developing practical suggestions, where possible, to account for nonlinear degrading response in the context of current seismic analysis procedures.

This report presents the findings and conclusions resulting from the literature search and focused analytical studies, and provides recommendations that can be used to improve both nonlinear static and nonlinear response history analysis modeling of strength and stiffness degradation for use in performance-based seismic design.

2. Literature Review

Past research has shown that in-cycle strength and stiffness degradation are real phenomena, and recent investigations confirm that the effects of in-cycle strength and stiffness degradation are critical in determining the possibility of lateral dynamic instability.

The body of knowledge is dominated by studies conducted within the last 20 years; however, relevant data on this topic extends as far back as the 1940s. A summary of background information taken from the literature is provided in Chapter 2. A comprehensive collection technical references on this subject is provided in Appendix A.

3. Focused Analytical Studies

To supplement the existing body of knowledge, focused analytical studies were performed using a set of eight nonlinear springs representing different types of inelastic hysteretic behavior. These basic spring types were used to develop 160 single-spring systems and 600 multi-spring systems with differing characteristics. Each system was subjected to incremental dynamic analysis with 56 ground motion records scaled to multiple levels of increasing intensity. The result is an extensive collection of data on nonlinear degrading response from over 2.6 million nonlinear response history analyses on single- and multi-spring systems.

Development of single- and multi-spring models is described in Chapter 3, analytical results are summarized in Chapter 4, and sets of analytical data are provided in the appendices. A Microsoft Excel visualization tool that was developed to view all available data from multi-spring studies is included on the CD accompanying this report.

4. Comparison with FEMA 440 Limitations on Strength for Lateral Dynamic Instability

In FEMA 440, a minimum strength requirement (R_{max}) was developed as an approximate measure of the need to further investigate the potential for lateral dynamic instability caused by in-cycle strength degradation and P-delta effects. To further investigate correlation between R_{max} and lateral dynamic instability, the results of this equation were compared to quantile incremental dynamic analysis (IDA) curves for selected multi-spring systems included in this investigation. Results indicate that values predicted by the FEMA 440 equation for R_{max} are variable, but generally plot between the median and 84th percentile results for lateral dynamic instability of the systems investigated. Observed trends indicate that an improved equation, in a form similar to R_{max}, could be developed as a more accurate (less variable) predictor of lateral dynamic instability for use in current nonlinear static analysis procedures.

5. Findings, Conclusions, and Recommendations

Findings, conclusions, and recommendations resulting from the literature review and focused analytical studies of this investigation are collected and summarized in Chapter 5, grouped into the following categories:

- Findings related to improved understanding of nonlinear degrading response and judgment in implementation of nonlinear analysis results in engineering practice.
- Recommended improvements to current nonlinear analysis procedures
- Suggestions for further study

6. Findings Related to Improved Understanding and Judgment

Results from focused analytical studies were used to identify predominant characteristics of median incremental dynamic analysis (IDA) curves and determine the effects of different degrading behaviors on the dynamic stability of structural systems. Observed practical ramifications from these studies are summarized below:

- Behavior of real structures can include loss of vertical-load-carrying capacity at lateral displacements that are significantly smaller than those associated with sidesway collapse. Use of the findings of this investigation with regard to lateral dynamic instability (sidesway

collapse) in engineering practice should include consideration of possible vertical collapse modes that could be present in the structure under consideration.

- Historically, the term "backbone curve" has referred to many different things. For this reason, two new terms have been introduced to distinguish between different aspects of hysteretic behavior. These are the *force-displacement capacity boundary*, and *cyclic envelope*.
- Nonlinear component parameters should be based on a force-displacement capacity boundary, rather than a cyclic envelope. Determining the force-displacement capacity boundary from test results using a single cyclic loading protocol can result in overly conservative predictions of maximum displacement.
- Observed relationships between selected features of the force-displacement capacity boundary and the resulting characteristics of median IDA curves support the conclusion that the nonlinear dynamic response of a system can be correlated to the parameters of the force-displacement capacity boundary of that system. Of particular interest is the relationship between global deformation demand and the intensity of the ground motion at lateral dynamic instability (collapse). Results indicate that it is possible to use nonlinear static procedures to estimate the potential for lateral dynamic instability of systems exhibiting in-cycle degradation.
- It is important to consider the dependence on period of vibration in conjunction with the effects of other parameters identified in this investigation. The generalized effect of any one single parameter can be misleading.
- It is important to recognize the level of uncertainty that is inherent in nonlinear analysis, particularly regarding variability in response due to ground motion uncertainty.
- In most cases the effects of in-cycle strength degradation dominate the nonlinear dynamic behavior of a system. This suggests that in many cases the effects of cyclic degradation can be neglected.
- Two situations in which the effects of cyclic degradation were observed to be important include: (1) short period systems; and (2) systems with very strong in-cycle strength degradation effects (very steep negative slopes and very large drops in lateral strength).

7. Improved Equation for Evaluating Lateral Dynamic Instability

An improved estimate for the strength ratio at which lateral dynamic instability might occur (R_{di}) was developed based on nonlinear regression of the extensive volume of data generated during this investigation. In performing this regression, results were calibrated to the median response of the SDOF spring systems studied in this investigation. Since the proposed equation for R_{di} has been calibrated to median response, use of this equation could eliminate some of the conservatism inherent in the current R_{max} limitation on use of nonlinear static procedures. Calibrated using the extensive volume of data generated during this investigation, use of this equation could improve the reliability of current nonlinear static procedures with regard to cyclic and in-cycle degradation.

Median response, however, implies a fifty percent chance of being above or below the specified value. Use of R_{di} in engineering practice should consider whether or not a median predictor represents an appropriate level of safety against the potential for lateral dynamic instability. If needed, a reduction factor could be applied to the proposed equation for R_{di} to achieve a higher level of safety on the prediction of lateral dynamic instability.

8. Simplified Nonlinear Dynamic Analysis Procedure

Focused analytical studies comparing force-displacement capacity boundaries to incremental dynamic analysis results led to the concept of a simplified nonlinear dynamic analysis procedure. In this procedure, a nonlinear static analysis is used to generate an idealized force-deformation curve (i.e., static pushover curve), which is then used as a force-displacement capacity boundary to constrain the hysteretic behavior of an equivalent SDOF oscillator. This SDOF oscillator is then subjected to incremental dynamic analysis, or approximate IDA results are obtained using the open source software tool, *Static Pushover 2 Incremental Dynamic Analysis*, SPO2IDA (Vamvatsikos and Cornell 2006). A Microsoft Excel version of the SPO2IDA application is included on the CD accompanying this report.

The procedure is simplified because only a SDOF oscillator is subjected to nonlinear dynamic analysis. Further simplification is achieved through the use of SPO2IDA, which avoids the computational effort associated with incremental dynamic analysis. This simplified procedure is shown to have several advantages over nonlinear static analysis procedures. Use of the procedure is explained in more detail in the example application contained in Appendix F.

9. Application of Results to Multiple-Degree-of-Freedom Systems

Multi-story buildings are more complex dynamic systems whose seismic response is more difficult to estimate than that of SDOF systems. Recent studies have suggested that it may be possible to estimate the collapse capacity of multiple-degree-of-freedom (MDOF) systems through dynamic analysis of equivalent SDOF systems. As part of the focused analytical work, preliminary studies of MDOF systems were performed. Results indicate that many of the findings for SDOF systems in this investigation (e.g., the relationship between force-displacement capacity boundary and IDA curves; the equation for R_{di}) may be applicable to MDOF systems.

Results of MDOF investigations are summarized in Appendix G. More detailed study of the application of these results to MDOF systems is recommended, and additional investigations are planned under a project funded by the National Institute of Standards and Technology (NIST).

10. Concluding Remarks

Using FEMA 440 as a starting point, this investigation has advanced the understanding of degradation and dynamic instability by:

- Investigating and documenting currently available empirical and theoretical knowledge on nonlinear cyclic and in-cycle strength and stiffness degradation, and their affects on the stability of structural systems
- Supplementing and refining the existing knowledge base with focused analytical studies

Results from this investigation have confirmed conclusions regarding degradation and dynamic instability presented in FEMA 440, provided updated information on modeling to differentiate between cyclic and in-cycle strength and stiffness degradation, and linked nonlinear dynamic response to major characteristics of component and system degrading behavior. This information will ultimately improve nonlinear modeling of structural components, improve the characterization of lateral dynamic instability, and reduce conservatism in current analysis procedures making it more cost-effective to strengthen existing buildings for improved seismic resistance in the future.

Table of Contents

List of Figures

List of Tables

Chapter 1
Introduction

Much of the nation's work regarding performance-based seismic design has been funded by the Federal Emergency Management Agency (FEMA), under its role in the National Earthquake Hazards Reduction Program (NEHRP). Prevailing practice for performance-based seismic design is based on FEMA 273, *NEHRP Guidelines for the Seismic Rehabilitation of Buildings* (FEMA, 1997) and its successor documents, FEMA 356, *Prestandard and Commentary for the Seismic Rehabilitation of Buildings* (FEMA, 2000), and ASCE/SEI Standard 41-06, *Seismic Rehabilitation of Existing Buildings* (ASCE, 2006b). This series of documents has been under development for over twenty years, and has been increasingly absorbed into engineering practice over that period.

The FEMA 440 report, *Improvement of Nonlinear Static Seismic Analysis Procedures* (FEMA, 2005), was commissioned to evaluate and develop improvements to nonlinear static analysis procedures used in prevailing practice. In FEMA 440, deviation between nonlinear static and nonlinear response history analyses was attributed to a number of factors including: (1) inaccuracies in the "equal displacement approximation" in the short period range; (2) dynamic P-delta effects and instability; (3) static load vector assumptions; (4) strength and stiffness degradation; (5) multi-degree of freedom effects; and (6) soil-structure interaction effects.

FEMA 440 identified and defined two types of degradation in inelastic single-degree-of-freedom oscillators. These included cyclic degradation and in-cycle degradation, as illustrated in Figure 1-1. Cyclic degradation was characterized by loss of strength and stiffness occurring in subsequent cycles. In-cycle degradation was characterized by loss of strength and negative stiffness occurring within a single cycle. This distinction was necessary because the consequences of cyclic degradation and in-cycle degradation were observed to be vastly different. In general, systems with cyclic degradation were shown to have stable dynamic response, while systems with severe in-cycle degradation were prone to dynamic instability, potentially leading to collapse.

Recommendations contained within FEMA 440 resulted in immediate improvement in nonlinear static analysis procedures, and were incorporated

in the development of ASCE/SEI 41-06. However, several difficult technical issues remained unresolved. These included the need for additional guidance and direction on: (1) expansion of component and global modeling to include nonlinear degradation of strength and stiffness; (2) improvement of simplified nonlinear modeling to include multi-degree of freedom effects; and (3) improvement of modeling to include soil and foundation structure interaction effects.

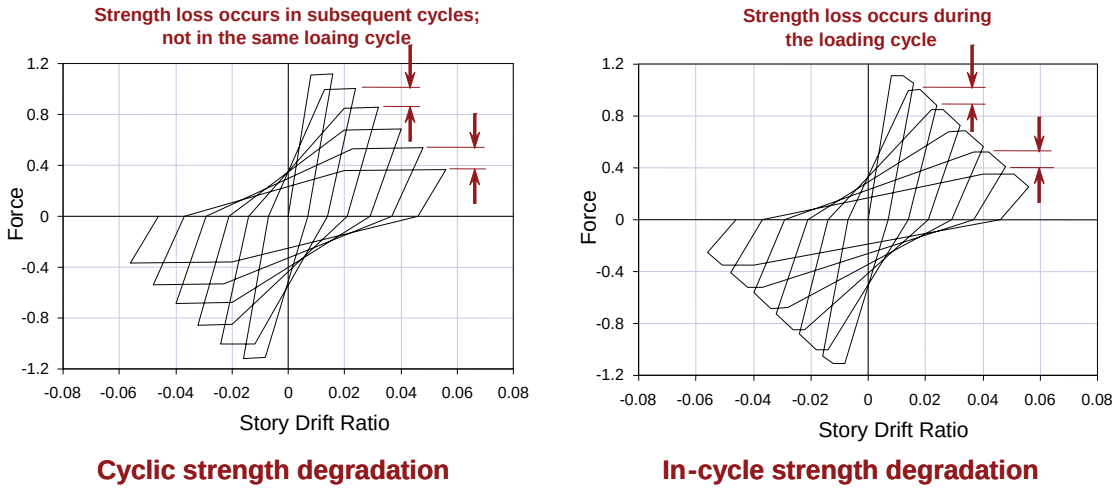

Figure 1-1 Types of degradation defined in FEMA 440.

1.1 Project Objectives

The Applied Technology Council (ATC) was commissioned by FEMA under the ATC-62 Project to further investigate the issue of component and global response to degradation of strength and stiffness. Using FEMA 440 as a starting point, the objectives of the project were to advance the understanding of degradation and dynamic instability by:

- Investigating and documenting currently available empirical and theoretical knowledge on nonlinear cyclic and in-cycle strength and stiffness degradation, and their affects on the stability of structural systems
- Supplementing and refining the existing knowledge base with focused analytical studies
- Developing practical suggestions, where possible, to account for nonlinear degrading response in the context of current seismic analysis procedures.

The result is an extensive collection of available research on component modeling of degradation, and a database of analytical results documenting the effects of a variety of parameters on the overall response of single-

degree-of-freedom systems with degrading components. This report presents the findings and conclusions resulting from focused analytical studies, and provides recommendations that can be used to improve both nonlinear static and nonlinear response history analysis modeling of strength and stiffness degradation for use in performance-based seismic design.

1.2 Scope of Investigation

The scope of the investigative effort included two primary activities. The first was to assemble and review currently available research on the effects of degrading nonlinear component properties on structural system response. The second was to augment this information with supplemental analytical data, where needed.

1.2.1 Literature Review

Work included an extensive review of existing research on hysteretic models that have been developed and used for modeling nonlinear response of structures, with an emphasis on those that have incorporated degradation of stiffness and strength. The review included theoretical and empirical investigations that have studied the effect of hysteretic behavior on seismic response. Interviews with selected researchers were also conducted.

The body of knowledge is dominated by studies conducted within the last 20 years; however, relevant data on this topic extends as far back as the 1940s. In summary, past research leads to the conclusion that in-cycle strength and stiffness degradation are real phenomena, and recent investigations confirm that the effects of in-cycle strength and stiffness degradation are critical in determining the possibility of lateral dynamic instability.

Only a small number of analytical studies and experimental tests have considered the dynamic loading effects of in-cycle strength and stiffness degradation. Most experimental studies to date have only considered individual components or individual subassemblies, and have not considered larger systems of components with mixed hysteretic behavior. There are only a few studies that have considered combined effects of strength, stiffness, period of vibration together with in-cycle degradation.

A summary of background information taken from the literature is provided in Chapter 2. A comprehensive collection and summary of technical references on the development, evolution, and applicability of various hysteretic models for use in nonlinear structural analysis is provided in Appendix A.

1.2.2 Focused Analytical Studies

To supplement the current state of knowledge, a program of nonlinear dynamic focused analytical studies was developed and implemented. The purpose of this program was to investigate the response of systems comprised of degrading components, test various characteristics of degrading component behavior, and identify their effects on the dynamic stability of a system.

The basis of the focused analytical studies is a set of eight nonlinear springs representing different types of inelastic hysteretic behavior:

- Typical gravity frame (e.g., steel)
- Non-ductile moment frame (e.g., steel or concrete)
- Ductile moment frame (e.g., steel or concrete)
- Stiff non-ductile system (e.g., concentric braced frame)
- Stiff and highly pinched non-ductile system (e.g., infill wall)
- Idealized elastic-perfectly-plastic system (for comparison)
- Limited-ductility moment frame (e.g., concrete)
- Non-ductile gravity frame (e.g., concrete)

Each spring was defined with a hysteretic model based on information available in the literature. While intended to be representative of realistic degrading response that has been observed to occur in some structural components, these idealized springs are not intended to be a detailed characterization of the mechanical behavior exclusively associated with any one specific structural component or structural assembly.

Individual springs were combined to approximate the behavior of more complex systems consisting of a mixture of subassemblies having different hysteretic characteristics. Combinations included gravity frame components working with various different primary lateral-force resisting components to approximate a range of possible building types encountered in practice. For each such combined system, variations in the relative contribution of individual springs to the initial stiffness and maximum lateral strength over a range of periods were considered. Development of single-degree-of-freedom (SDOF) models used in focused analytical studies is described in Chapter 3.

Extensive parametric studies varying the strength, stiffness, period, and post-elastic properties were conducted on each component spring and combined system using Incremental Dynamic Analysis (IDA). Results of over 2.6 million nonlinear response history analyses are summarized in Chapter 4.

A limited study of multiple-degree-of-freedom (MDOF) systems was also conducted. This effort compared the results of nonlinear dynamic analyses of MDOF buildings performed by others to analytical results for SDOF representations of the same systems. The purpose was to investigate the extent to which results from nonlinear static analyses might be combined with dynamic analyses of SDOF systems to estimate the global response of MDOF systems. Preliminary MDOF investigations are described in Appendix G. Additional MDOF investigations are planned under a project funded by the National Institute of Standards and Technology (NIST).

1.3 Report Organization and Content

Chapter 1 introduces the project context, objectives, and scope of the investigation.

Chapter 2 provides background information related to modeling of component hysteretic behavior, summarizes results of past studies, and introduces new terminology.

Chapter 3 describes the development of SDOF models, and explains the analytical procedures used in the conduct of focused analytical studies.

Chapter 4 summarizes the results of focused analytical studies on single-spring and multi-spring systems, compares results to recommendations contained in FEMA 440, and explains the development of a new equation measuring the potential for lateral dynamic instability.

Chapter 5 collects and summarizes the findings, conclusions, and recommendations resulting from this investigation related to improved understanding of nonlinear degrading response and judgment in implementation of nonlinear analysis results in engineering practice, improvements to current nonlinear analysis procedures, and suggestions for further study.

Appendix A provides a comprehensive collection and summary of technical references on the development, evolution, and applicability of various hysteretic models for use in nonlinear structural analysis.

Appendix B contains plots of selected incremental dynamic analysis results for single-spring systems.

Appendix C contains normalized plots of selected incremental dynamic analysis results for multi-spring systems.

Appendix D contains non-normalized plots of selected incremental dynamic analysis results for multi-spring systems.

Appendix E explains the concepts of uncertainty and fragility, how incremental dynamic analysis results can be converted into fragilities, and how to use this information to calculate estimates of annualized probability for limit states of interest.

Appendix F provides an example application of a simplified nonlinear dynamic analysis procedure, including quantitative evaluation of alternative retrofit strategies and development of probabilistic estimates of performance using the concepts outlined in Appendix E.

Appendix G describes a set of preliminary studies of MDOF systems comparing results of MDOF analyses with results from equivalent SDOF representations of the systems, and provides recommendations for additional MDOF studies.

A compact disc (CD) accompanying this report provides electronic files of the report and appendices in PDF format, an electronic visualization tool in Microsoft Excel format that can be used to view the entire collection of multi-spring incremental dynamic analysis results, and the *Static Pushover 2 Incremental Dynamic Analysis* (SPO2IDA) software tool in Microsoft Excel format (Vamvatsikos and Cornell, 2006) that can be used to estimate the dynamic response of systems based on idealized force-displacement (static pushover) curves.

Chapter 2
Background Concepts

This chapter provides background information on modeling of component hysteretic behavior. It summarizes how various types of hysteretic behavior have been investigated in past studies, and explains how these behaviors have been observed to affect seismic response. It introduces new terminology, and explains how the new terms are related to observed differences in nonlinear dynamic response.

2.1 Effects of Hysteretic Behavior on Seismic Response

Many hysteretic models have been proposed over the years with the purpose of characterizing the mechanical nonlinear behavior of structural components (e.g., members and connections) and estimating the seismic response of structural systems (e.g., moment frames, braced frames, shear walls). Available hysteretic models range from simple elasto-plastic models to complex strength and stiffness degrading curvilinear hysteretic models. This section presents a summary of the present state of knowledge on hysteretic models, and their influence on the seismic response of structural systems. A comprehensive summary of technical references on the development, evolution, and applicability of various hysteretic models is presented in Appendix A.

2.1.1 Elasto-Plastic Behavior

In the literature, most studies that have considered nonlinear behavior have used non-degrading hysteretic models, or models in which the lateral stiffness and the lateral yield strength remain constant throughout the duration of loading. These models do not incorporate stiffness or strength degradation when subjected to repeated cyclic load reversals. The simplest and most commonly used non-deteriorating model is an elasto-plastic model in which system behavior is linear-elastic until the yield strength is reached (Figure 2-1). At yield, the stiffness switches from elastic stiffness to zero stiffness. During unloading cycles, the stiffness is equal to the loading (elastic) stiffness.

Early examples of the use of elasto-plastic models include studies by Berg and Da Deppo (1960), Penzien (1960a, 1960b), and Veletsos and Newmark (1960). The latter study was the first one to note that peak lateral

displacements of moderate and long-period single-degree-of-freedom (SDOF) systems with elasto-plastic behavior were, on average, about the same as that of linear elastic systems with the same period of vibration and same damping ratio. Their observations formed the basis of what is now known as the "equal displacement approximation." This widely-used approximation implies that the peak displacement of moderate and long-period non-degrading systems is proportional to the ground motion intensity, meaning that if the ground motion intensity is doubled, the peak displacement will be on average, approximately twice as large.

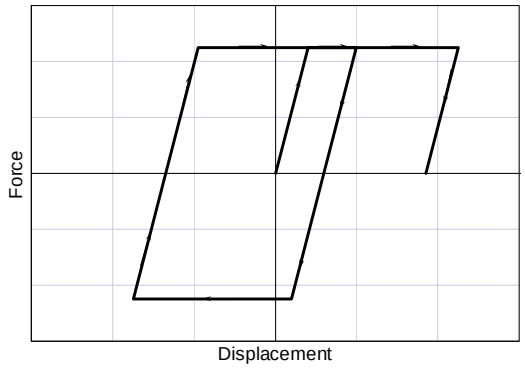

Figure 2-1 Elasto-plastic non-degrading piecewise linear hysteretic model.

Veletsos and Newmark also observed that peak lateral displacement of short-period SDOF systems with elasto-plastic behavior were, on average, larger than those of linear elastic systems, and increases in peak lateral displacements were larger than the increment in ground motion intensity. Thus, the equal displacement approximation was observed to be less applicable to short-period structures.

Using many more ground motions, recent studies have corroborated some of the early observations by Veletsos, identified some of the limitations in the equal displacement approximation, and provided information on record-to-record variability (Miranda, 1993, 2000; Ruiz-Garcia and Miranda, 2003; Chopra and Chintanapakdee, 2004). These studies have shown that, in the short-period range, peak inelastic system displacements increase with respect to elastic system displacements as the period of vibration decreases and as the lateral strength decreases. These observations formed the basis of the improved displacement modification coefficient C_1, which accounts for the effects of inelastic behavior in the coefficient method of estimating peak displacements, as documented in FEMA 440 *Improvement of Nonlinear Static Seismic Analysis Procedures* (FEMA, 2005).

2.1.2 Strength-Hardening Behavior

Another commonly used non-degrading hysteretic model is a strength-hardening model, which is similar to the elasto-plastic model, except that the post-yield stiffness is greater than zero (Figure 2-2). Early applications of bilinear strength-hardening models include investigations by Caughey (1960a, 1960b) and Iwan (1961). Positive post-yield stiffness is also referred to as "strain hardening" because many materials exhibit gains in strength (harden) when subjected to large strain levels after yield. Strength hardening in components, connections, and systems after initial yield is also caused by eventual mobilization of a full member crossection, or sequential yielding of the remaining elements in a system. This is typically the most important source of strength hardening observed in a structural system.

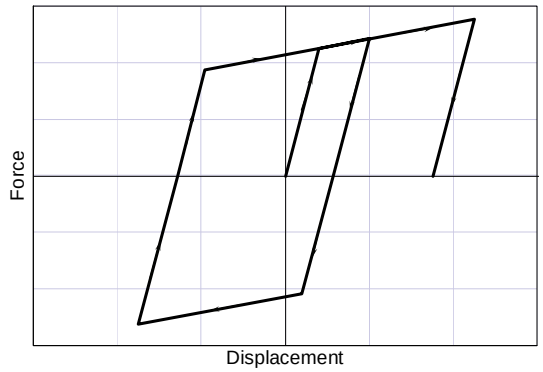

Figure 2-2 Strength-hardening non-degrading piecewise linear hysteretic model.

Although many studies have considered elasto-plastic and bilinear strength-hardening behavior, it was not until recently that comprehensive statistical studies were conducted to systematically quantify differences in peak displacements using a wide range of periods of vibration, a wide range of post-elastic stiffnesses, and large numbers of ground motions. Several recent studies have provided quantitative information on the average effects of positive post-yield stiffness on response, and on the variability in response for different ground motion records. They are in agreement that, for moderate and long-period structures, the presence of a positive post-elastic stiffness leads to relatively small (less than 5%) reductions in peak displacement (Ruiz-Garcia and Miranda, 2003; Chopra and Chintanapakdee, 2004). The magnitude of the reduction varies based on the strength of the system and period of vibration.

System strength is often characterized by a parameter, *R*, defined as the ratio between the strength that would be required to keep the system elastic for a

given intensity of ground motion, S_{aT}, and the lateral yield strength of the system, F_y:

$$R = \frac{S_{aT}}{F_y / W} = \frac{S_{aT} g}{F_y} \tag{2-1}$$

where S_{aT} is expressed as a percentage of gravity. This R factor is related to, but not the same as, the response-modification coefficient used in code-based equivalent lateral force design procedures.

For weaker systems (systems with higher values of R), the reduction in response is greater (more beneficial). For short-period systems, the presence of a positive post-elastic stiffness can lead to significant reductions in peak lateral displacements.

Other recent studies have shown that a positive post-elastic stiffness can have a very large effect in other response parameters. In particular, MacRae and Kawashima (1997), Kawashima et al., (1998) Pampanin et al. (2002), Ruiz-Garcia and Miranda, (2006a) have shown that small increments in post-yield stiffness can lead to substantial reductions in residual drift in structures across all period ranges.

2.1.3 Stiffness-Degrading Behavior

Many structural components and systems will exhibit some level of stiffness degradation when subjected to reverse cyclic loading. This is especially true for reinforced concrete components subjected to several large cyclic load reversals. Stiffness degradation in reinforced concrete components is usually the result of cracking, loss of bond, or interaction with high shear or axial stresses. The level of stiffness degradation depends on the characteristics of the structure (e.g., material properties, geometry, level of ductile detailing, connection type), as well as on the loading history (e.g., intensity in each cycle, number of cycles, sequence of loading cycles).

Figure 2-3 shows three examples of stiffness-degrading models. In the first model, the loading and unloading stiffness is the same, and the stiffness degrades as displacement increases. In the second model the loading stiffness decreases as a function of the peak displacement, but the unloading stiffness is kept constant and equal to the initial stiffness. In the third model, both the loading and unloading stiffnesses degrade as a function of peak displacement, but they are not the same.

In order to evaluate the effects of stiffness degradation, many studies have compared the peak response of stiffness-degrading systems to that of elasto-plastic and bilinear strength-hardening systems (Clough 1966; Clough and

Johnston 1966; Chopra and Kan, 1973; Powel and Row, 1976; Mahin and Bertero, 1976; Riddell and Newmark, 1979; Newmark and Riddell, 1980; Iwan 1980; Otani, 1981; Nassar and Krawinkler 1991; Rahnama and Krawinkler, 1993; Shi and Foutch, 1997; Foutch and Shi, 1998; Gupta and Krawinkler, 1998; Gupta and Kunnath, 1998; Medina 2002; Medina and Krawinkler, 2004; Ruiz-Garcia and Miranda, 2005).

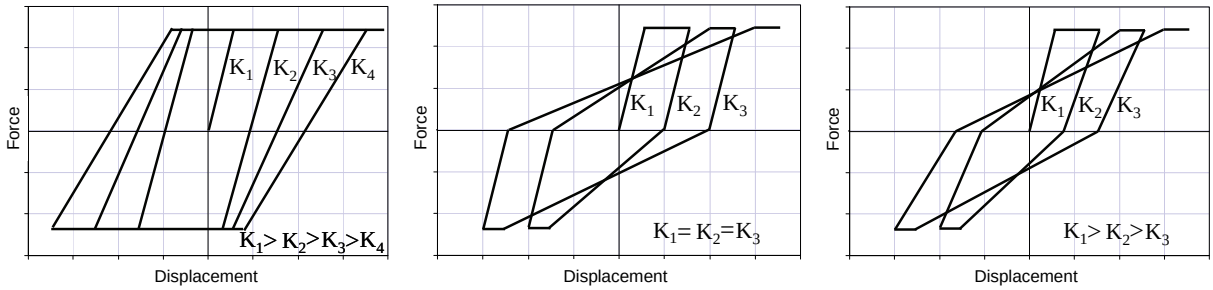

Figure 2-3 Three examples of stiffness-degrading piecewise linear hysteretic models.

These studies have concluded that, in spite of significant reductions in lateral stiffness and hysteretic energy dissipation capacity (area enclosed within hysteresis loops), moderate and long-period systems with stiffness-degrading behavior experience peak displacements that are, on average, similar to those of structures with elasto-plastic or bilinear strength-hardening hysteretic behavior. In some cases, peak displacements can even be slightly smaller. This observation suggests that it is possible to use simpler hysteretic models that do not incorporate stiffness degradation to estimate lateral displacement demands for moderate and long-period structures (systems with fundamental periods longer than 1.0s).

These same studies, however, have concluded that short-period structures with stiffness degradation experience peak displacements that are, on average, larger than those experienced by systems with elasto-plastic or bilinear strength-hardening hysteretic behavior. Differences in peak displacements between stiffness-degrading and non-degrading systems increase as the period of vibration decreases and as the lateral strength decreases.

The above studies examined the effects of stiffness degradation on structures subjected to ground motions recorded on rock or firm soil sites. Ruiz-Garcia and Miranda (2006b) examined the effects of stiffness degradation on structures subjected to ground motions recorded on soft soil sites. This study concluded that the effects of stiffness degradation are more important for structures built on soft soil, especially for structures with periods shorter than the predominant period of the ground motion.

2.1.4 Pinching Behavior

Structural components and connections may exhibit a hysteretic phenomenon called pinching when subjected to reverse cyclic loading (Figure 2-4). Pinching behavior is characterized by large reductions in stiffness during reloading after unloading, along with stiffness recovery when displacement is imposed in the opposite direction.

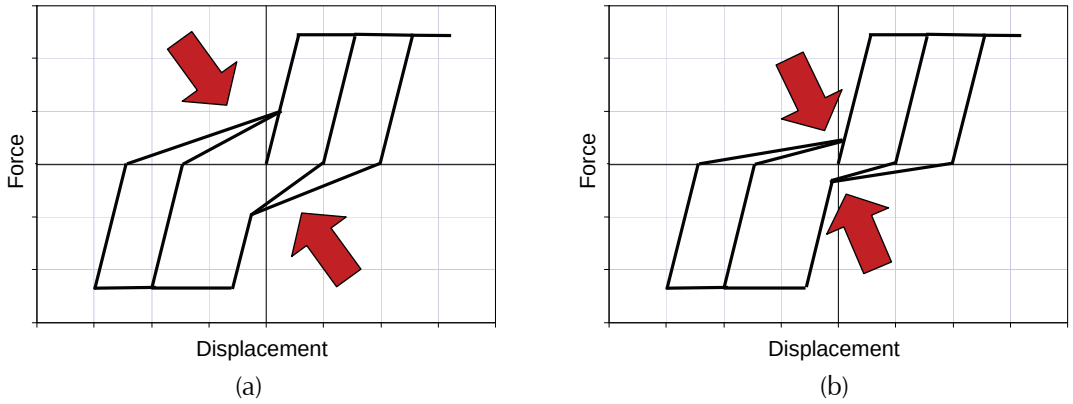

Figure 2-4 Examples of hysteretic models with: (a) moderate pinching behavior; and (b) severe pinching behavior.

Pinching behavior is particularly common in reinforced concrete components, wood components, certain types of masonry components, and some connections in steel structures. In reinforced concrete, pinching is typically produced by opening of cracks when displacement is imposed in one direction. Partial stiffness recovery occurs when cracks are closed during displacements imposed in the other direction. In wood structures pinching is primarily caused by opening and closing of gaps in framing elements due to nail pullout. Pinching also occurs as a result of opening and closing of flexural cracks in reinforced masonry, opening and closing of gaps between masonry infill and the surrounding structural frame, and opening and closing of gaps between plates in steel end-plate connections. The level of pinching depends on the characteristics of the structure (e.g., material properties, geometry, level of ductile detailing, and connections), as well as the loading history (e.g., intensity in each cycle, number of cycles, and sequence of loading cycles).

Several studies have shown that, for moderate and long-period systems, pinching alone or in combination with stiffness degradation has only a small affect on peak displacement demands, as long as the post-yield stiffness remains positive (Otani, 1981; Nassar and Krawinkler 1991; Rahnama and Krawinkler, 1993; Shi and Foutch, 1997; Foutch and Shi, 1998; Gupta and

Krawinkler, 1998; Gupta and Kunnath, 1998; Medina 2002; Medina and Krawinkler, 2004; Ruiz-Garcia and Miranda, 2005).

These and other studies have shown that moderate and long-period systems, with up to 50% reduction in hysteretic energy dissipation capacity due to pinching, experience peak displacements that are, on average, similar to those of structures with elasto-plastic or bilinear strength-hardening hysteretic behavior. This observation is particularly interesting because it is contrary to the widespread notion that structures with elasto-plastic or bilinear behavior exhibit better performance than structures with pinching behavior because of the presence of additional hysteretic energy dissipation capacity.

These same studies, however, have also shown that short-period structures with pinching behavior experience peak displacements that tend to be larger than those experienced by systems with elasto-plastic or bilinear strength-hardening hysteretic behavior. Differences in peak displacements increase as the period of vibration decreases and as the lateral strength decreases.

2.1.5 Cyclic Strength Degradation

Structural components and systems may experience reductions in strength generically referred to as strength degradation or strength deterioration (Figure 2-5). One of the most common types of strength degradation is cyclic strength degradation in which a structural component or system experiences a reduction in lateral strength as a result of cyclic load reversals.

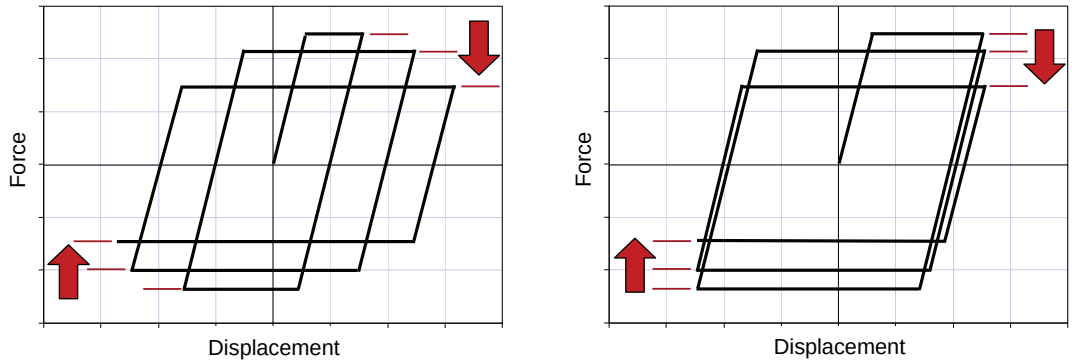

Figure 2-5 Examples of cyclic strength degradation: (a) due to increasing inelastic displacement; and (b) due to repeated cyclic displacement

In cyclic strength degradation, reductions in lateral strength occur after the loading has been reversed, or during subsequent loading cycles. Cyclic reductions in lateral strength are a function of the level of peak displacement experienced in the system (Park, Reinhorn and Kunnath, 1987; Rahnama and

Krawinkler, 1993). This is illustrated in Figure 2-5(a), which shows an elasto-plastic system experiencing strength degradation in subsequent loading cycles as the level of inelastic displacement increases. Hysteretic models that incorporate this type of strength degradation typically specify the reduction in strength as a function of the ductility ratio, which is taken as the ratio of peak deformation to yield deformation.

Cyclic strength degradation can also occur in subsequent cycles even if the level of inelastic displacement is not being increased (Park, Reinhorn and Kunnath, 1987; Rahnama and Krawinkler, 1993). This is illustrated in Figure 2-5(b), which shows an elasto-plastic system experiencing cyclic strength degradation as a result of a single level of inelastic displacement that is imposed a number of times. The reduction in lateral strength increases as the number of cycles increases. Hysteretic models that incorporate this type of strength degradation (Park, Reinhorn and Kunnath, 1987; Rahnama and Krawinkler, 1993; Mostaghel 1998, 1999; Sivaselvan and Reinhorn 1999, 2000) typically specify the reduction in strength as a function of the total hysteretic energy demand imposed on the system, taken as the area enclosed by the hysteresis loops.

Most structural systems exhibit a combination of the types of cyclic strength degradation shown in Figure 2-5. Several hysteretic models that incorporate both types of cyclic strength degradation have been developed (Park and Ang, 1985; Park, Reinhorn and Kunnath, 1987; Rahnama and Krawinkler, 1993; Valles et al., 1996; Shi and Foutch, 1997; Foutch and Shi, 1998; Gupta and Krawinkler, 1998;Gupta and Kunnath, 1998; Pincheira, Dotiwala, and D' Souza 1999; Medina 2002; Medina and Krawinkler, 2004; Mostaghel 1998, 19990; Sivaselvan and Reinhorn 1999, 2000; Chenouda, and Ayoub, 2007).

Many of these same investigators have compared the peak response of systems with cyclic strength degradation to that of elasto-plastic and bilinear strength-hardening systems. In moderate and long-periods systems, the effects of cyclic strength degradation have been shown to be very small, and in many cases can be neglected, even with reductions in strength of 50% or more. The reason for this can be explained using early observations from Veletsos and Newmark (1960), which concluded that peak displacement demands in moderate and long-period systems were not sensitive to changes in yield strength. This conclusion logically extends to moderate and long-period systems that experience cyclic changes (reductions) in lateral strength during loading.

In short-period structures, however, studies have shown that cyclic strength degradation can lead to significant increases in peak displacement demands.

This observation can also be explained by results from Veletsos and Newmark (1960), which concluded that peak displacement demands in short-period systems are very sensitive to changes in yield strength. This conclusion logically extends to short-period systems that experience cyclic changes (reductions) in lateral strength during loading.

2.1.6 Combined Stiffness Degradation and Cyclic Strength Degradation

Several recent studies have examined the effects of stiffness degradation in combination with cyclic strength degradation (Gupta and Kunnath, 1998; Song and Pincheira, 2000; Medina 2002; Medina and Krawinkler, 2004; Ruiz-Garcia and Miranda, 2005; Chenouda, and Ayoub, 2007). Examples of these behaviors are illustrated in Figure 2-6. Figure 2-6a shows a system with moderate stiffness and cyclic strength degradation (MSD), and Figure 2-6b shows a system with severe stiffness and cyclic strength degradation (SSD). In these systems, lateral strength is reduced as a function of both the peak displacement demand as well as the hysteretic energy demand on the system.

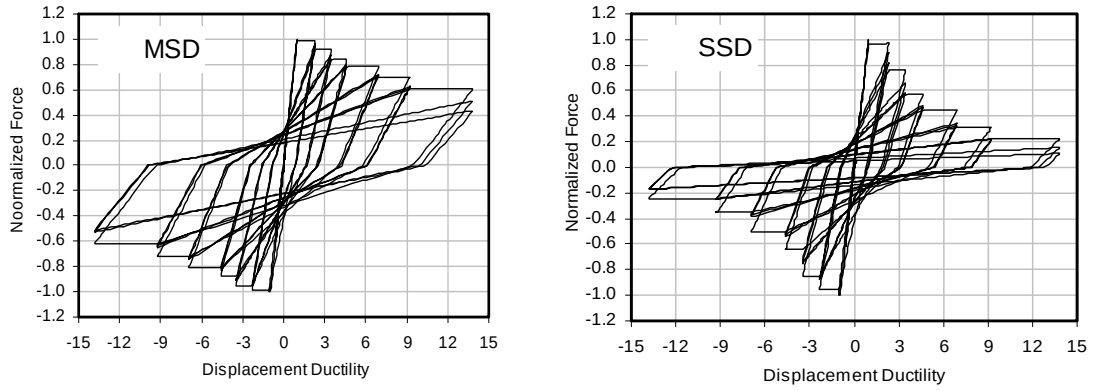

(a) (b)

Figure 2-6 Hysteretic models combining stiffness degradation and cyclic strength degradation: (a) moderate stiffness and cyclic strength degradation; and (b) severe stiffness and cyclic strength degradation (Ruiz-Garcia and Miranda, 2005).

These studies have shown that, for moderate and long-period systems with combined stiffness and cyclic strength degradation, peak displacements are, on average, similar to those experienced by elasto-plastic or bilinear strength-hardening systems. These effects are only observed to be significant for short-period systems (systems with periods of vibration less than 1.0s).

2.1.7 In-Cycle Strength Degradation

In combination with stiffness degradation, structural components and systems may experience in-cycle strength degradation (Figure 2-7). In-cycle

strength degradation is characterized by a loss of strength within the same cycle in which yielding occurs. As additional lateral displacement is imposed, a smaller lateral resistance is developed. This results in a negative post-yield stiffness within a given cycle.

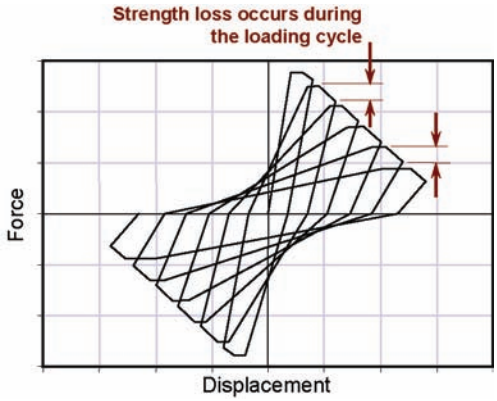

Figure 2-7 In-cycle strength degradation.

In-cycle strength degradation can occur as a result of geometric nonlinearities (P-delta effects), material nonlinearities, or a combination of these. In reinforced concrete components, material nonlinearities that can lead to in-cycle strength degradation include concrete crushing, shear failure, buckling or fracture of longitudinal reinforcement, and splice failures. In steel components, material nonlinearities that can lead to in-cycle strength degradation include buckling of bracing elements, local buckling in flanges of columns or beams, and fractures of bolts, welds, or base materials.

2.1.8 Differences Between Cyclic and In-Cycle Strength Degradation

FEMA 440 identified the distinction between cyclic and in-cycle degradation to be very important because the consequences of each were observed to be vastly different. Dynamic response of systems with cyclic strength degradation is generally stable, while in-cycle strength degradation can lead to lateral dynamic instability (i.e., collapse) of a structural system.

Figure 2-8 compares the hysteretic behavior of two systems subjected to the loading protocol shown in Figure 2-9. This loading protocol comprises six full cycles (twelve half-cycles) with a linearly increasing amplitude of 0.8% drift in each cycle. The system in Figure 2-8a has cyclic degradation and the system in Figure 2-8b has in-cycle degradation. When subjected to this loading protocol, both hysteretic models exhibit similar levels of strength and stiffness degradation, and similar overall behavior. Their behavior under different loading protocols, however, can be significantly different.

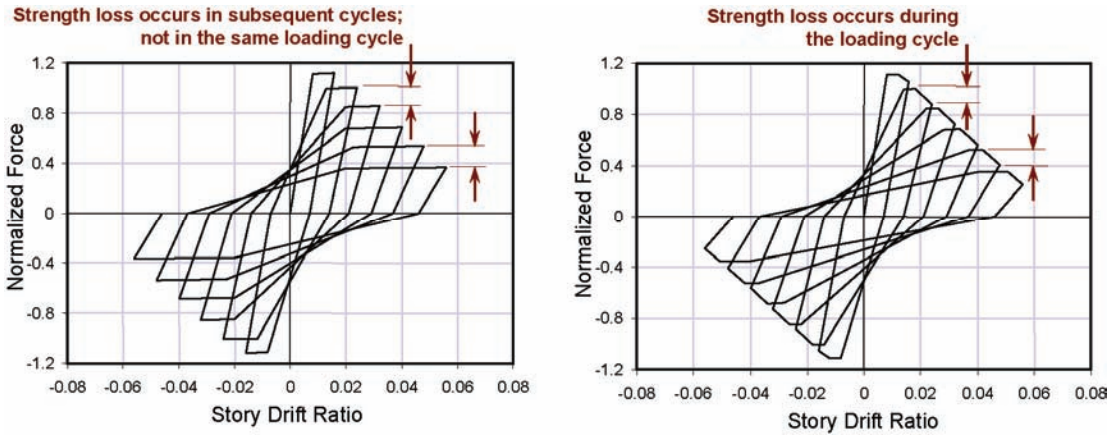

(a) (b)

Figure 2-8 Hysteretic behavior for models subjected to Loading Protocol 1 with: (a) cyclic strength degradation; and (b) in-cycle degradation.

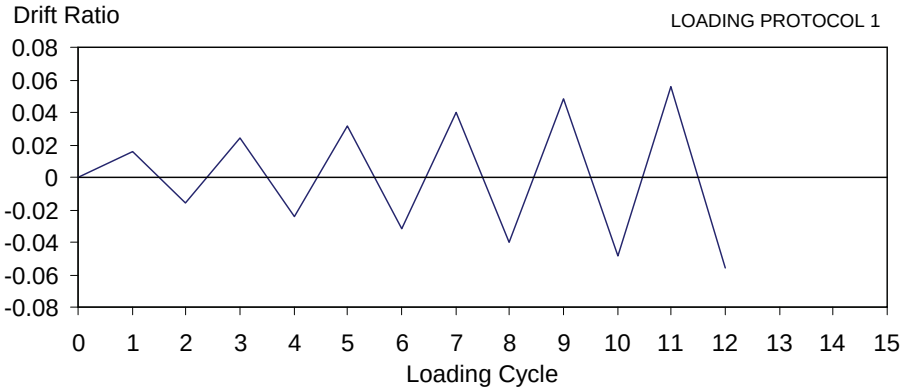

Figure 2-9 Loading Protocol 1 used to illustrate the effects of cyclic and in-cycle strength degradation.

A second loading protocol, shown in Figure 2-10, is identical to the first protocol through four half-cycles, but during the fifth half-cycle it continues to impose additional lateral displacement until a drift ratio of 7.0% is reached.

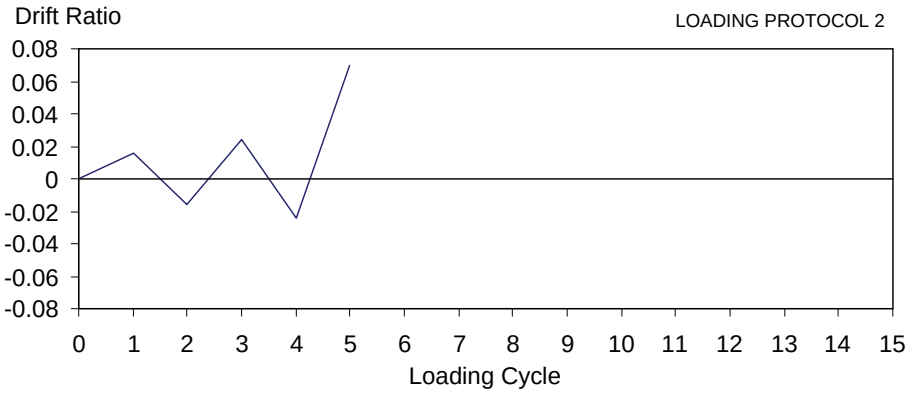

Figure 2-10 Loading Protocol 2 used to illustrate the effects of cyclic and in-cycle strength degradation.

Figure 2-11 compares the hysteretic behavior of both systems subjected to the second loading protocol. Initially, the responses are similar. During the fifth half-cycle, however, the responses diverge. The model with cyclic degradation (Figure 2-11a) is able to sustain lateral strength without loss as the drift ratio increases. In contrast, the model with in-cycle degradation (Figure 2-11b) experiences a rapid loss in strength as the drift ratio increases. While the model with cyclic strength degradation remains stable, the model with in-cycle strength degradation becomes unstable after losing lateral resistance.

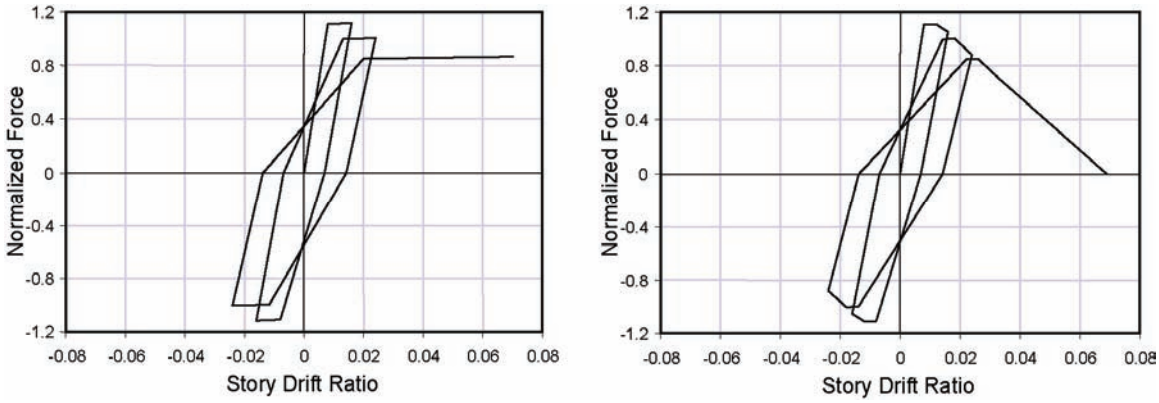

Figure 2-11 Hysteretic behavior for models subjected to Loading Protocol 2 with: (a) cyclic strength degradation; and (b) in-cycle degradation.

Figure 2-12 shows the displacement time histories for these same two systems when subjected to the north-south component of the Yermo Valley ground motion of the 1992 Landers Earthquake. The system with cyclic strength degradation (Figure 2-12a) undergoes a large peak drift ratio during the record, experiences a residual drift at the end of the record, and yet remains stable over the duration of the record. In contrast, the system with in-cycle degradation (Figure 2-12b) undergoes a similar peak drift ratio during the record, but ratchets further in one direction in subsequent yielding cycles, and eventually experiences lateral dynamic instability (collapse).

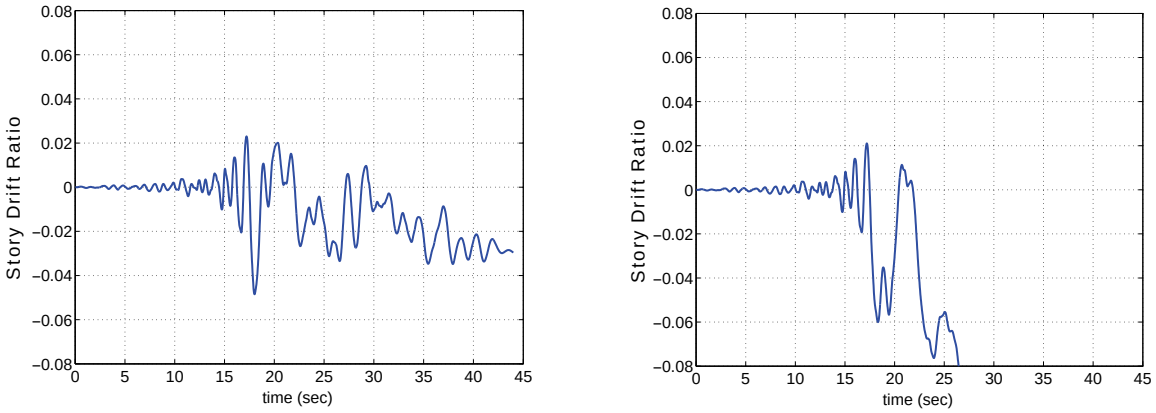

Figure 2-12 Displacement time histories for models subjected to the 1992 Landers Earthquake with: (a) cyclic strength degradation; and (b) in-cycle strength degradation.

2.2 Concepts and Terminology

Historically, the term *backbone curve* has referred to many different things. It has been used, for example, to describe limitations on the force-deformation behavior of structural components, force-displacement plots from nonlinear static pushover analyses of structural systems, curves enveloping the force-displacement response of structural components undergoing cyclic testing, and curves tracing the force-displacement response of structural components undergoing monotonic testing.

In the case of component modeling, parameters taken from one definition of a backbone curve versus another are not interchangeable, and their incorrect usage can have a significant affect on the predicted nonlinear response. For this reason, two new terms are introduced to distinguish between different aspects of hysteretic behavior. These are the *force-displacement capacity boundary*, and *cyclic envelope*.

2.2.1 Force-Displacement Capacity Boundary

Several recent models have been developed to incorporate various types of degrading phenomena (Kunnath, Reinhorn and Park, 1990; Kunnath, Mander and Fang, 1997; Mostaghel 1998, 19990; Sivaselvan and Reinhorn 1999, 2000; Ibarra, Medina, Krawinkler, 2005; Chenouda and Ayoub, 2007). A common feature in all these degrading models is that they start by defining the maximum strength that a structural member can develop at a given level of deformation. This results in an effective "boundary" for the strength of a member in force-deformation space, termed the *force-displacement capacity boundary*.

Figure 2-13 shows examples of two such boundaries commonly used in structural analysis of degrading components. These curves resemble the conceptual force-displacement relationship used to express component modeling and acceptability criteria in ASCE/SEI 41-06 *Seismic Rehabilitation of Existing Buildings* (ASCE, 2006b), commonly referred to as "backbones."

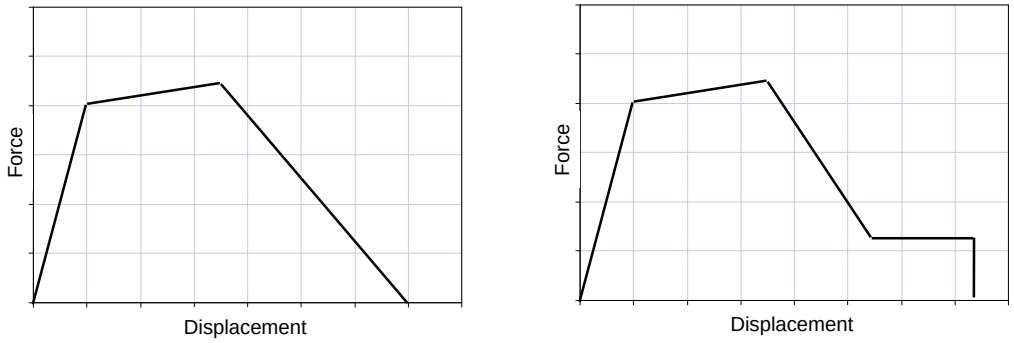

Figure 2-13 Examples of commonly used force-displacement capacity boundaries.

A cyclic load path cannot cross a force-displacement capacity boundary. If a member is subjected to increasing deformation and the boundary is reached, then the strength that can be developed in the member is limited and the response must continue along the boundary. This behavior is in-cycle strength degradation, and is shown in Figure 2-14. Note that only displacement excursions intersecting portions of the capacity boundary with a negative slope will result in in-cycle strength degradation.

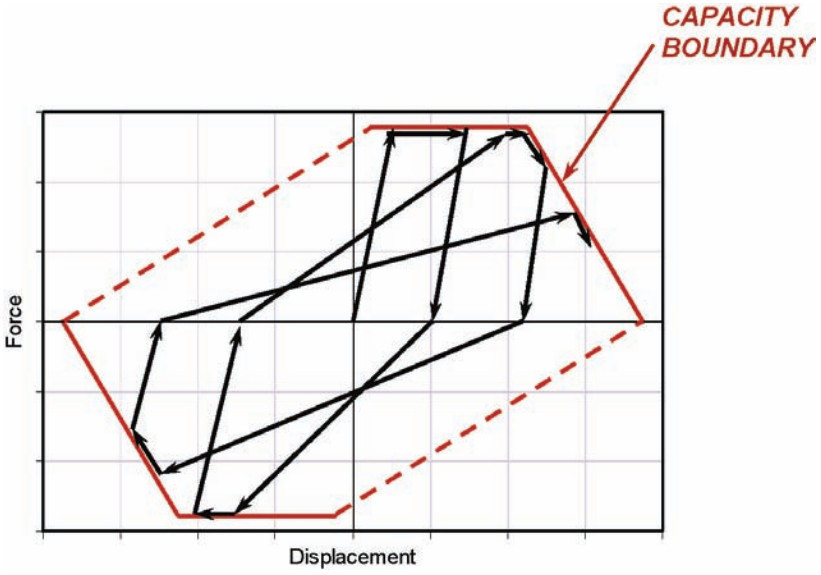

Figure 2-14 Interaction between the cyclic load path and the force-displacement capacity boundary.

In most cases, the force-displacement capacity boundary will not be static. More advanced models consider that the force-displacement capacity boundary will degrade (move inward) as a result of cyclic degradation (Figure 2-15). In some cases, it is also possible for the boundary to move outward due to cyclic strain hardening, such as in the case of structural steel elements subjected to large strains, but this behavior is not considered here.

In order to define the cyclic behavior of a component model, one must define where the force-displacement capacity boundary begins, and how it degrades under cyclic loading. In the absence of cyclic strain hardening, the initial force-displacement capacity boundary is simply the monotonic response of a component. Accordingly, the ideal source for estimating the parameters of the initial force-displacement capacity boundary comes from monotonic tests.

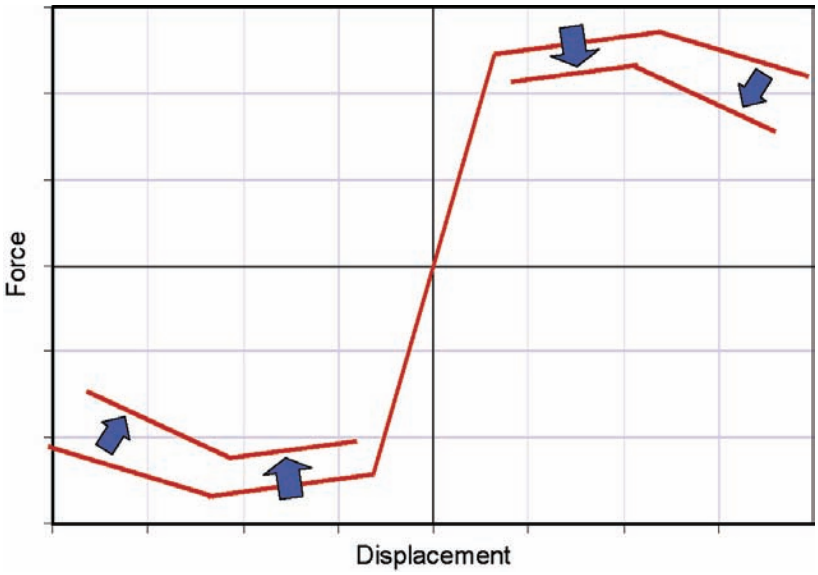

Figure 2-15 Degradation of the force-displacement capacity boundary.

Once the initial capacity boundary is defined, then cyclic degradation parameters must be estimated based on the results of cyclic tests. The use of several cyclic protocols is desirable to ensure that the calibrated component model is general enough to represent component response under any type of loading. This requires the availability of multiple identical specimens that are tested under several different loading protocols, which is a significant undertaking, and is rarely done.

When utilizing existing test data to calibrate a component model, it is uncommon to find sets of test data that include both monotonic and cyclic tests on identical specimens. It is even more uncommon to find sets of data that include monotonic tests and cyclic tests using multiple loading protocols

on identical specimens. As such, there are only a small number of cases in which this kind of data exists (Tremblay et al., 1997; El-Bahy, 1999; Ingham et al., 2001; Uang et al., 2000; Uang et al., 2003).

Most existing data is based only on a single cyclic loading protocol. In such cases, cyclic degradation can be approximated directly from the test data. In the absence of monotonic test data, the initial force-displacement capacity boundary must be extrapolated from the cyclic data (since the monotonic response is unknown). Considerable judgment must be exercised in extrapolating an initial force-displacement capacity boundary because there may be several combinations of initial parameters and cyclic degradation parameters that result in good agreement with the observed cyclic test data. Such an approach has been used by Haselton et al. (2007) for reinforced concrete components and Lignos (2008) for steel components.

2.2.2 Cyclic Envelope

A *cyclic envelope* is a force-deformation curve that envelopes the hysteretic behavior of a component or assembly that is subjected to cyclic loading. Figure 2-16 shows a cyclic envelope, which is defined by connecting the peak force responses at each displacement level.

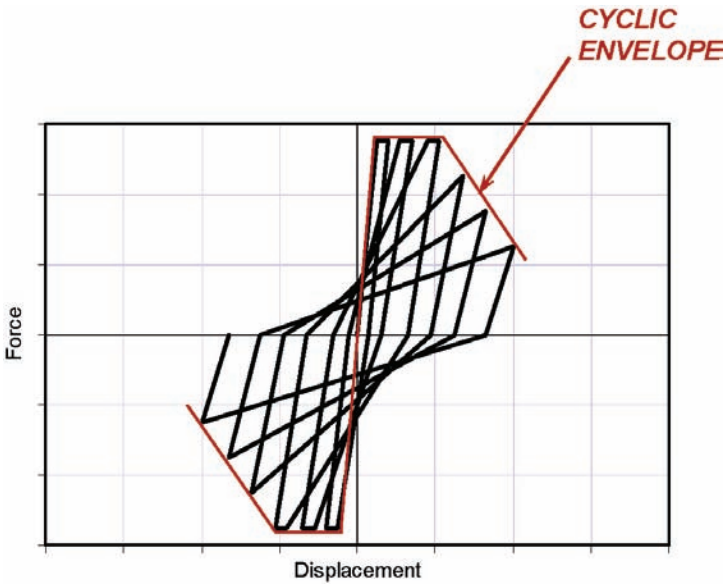

Figure 2-16 Example of a cyclic envelope.

Where loading protocols have included multiple cycles at each displacement increment, a different curve (often referred to as cyclic "backbone") has been defined based on the force at either the second or third cycle at each displacement level. Such a definition was included in FEMA 356 *Prestandard and Commentary for the Seismic Rehabilitation of Buildings*

(FEMA, 2000). In ASCE/SEI 41-06 (with Supplement No. 1) this has been changed to be more consistent with the concept of a cyclic envelope, as described above.

2.2.3 Influence of Loading Protocol on the Cyclic Envelope

The characteristics of a cyclic envelope are strongly influenced by the points at which unloading occurs in a test, and are therefore strongly influenced by the loading protocol that was used in the experimental program. Studies by Takemura and Kawashima (1997) illustrate the influence that the loading protocol can have on the characteristics of the cyclic envelope. In these studies, six nominally identical reinforced concrete bridge piers were tested using six different loading protocols, yielding six significantly different hysteretic behaviors. The loading protocols and resulting hysteretic plots are shown in Figure 2-17 through Figure 2-19.

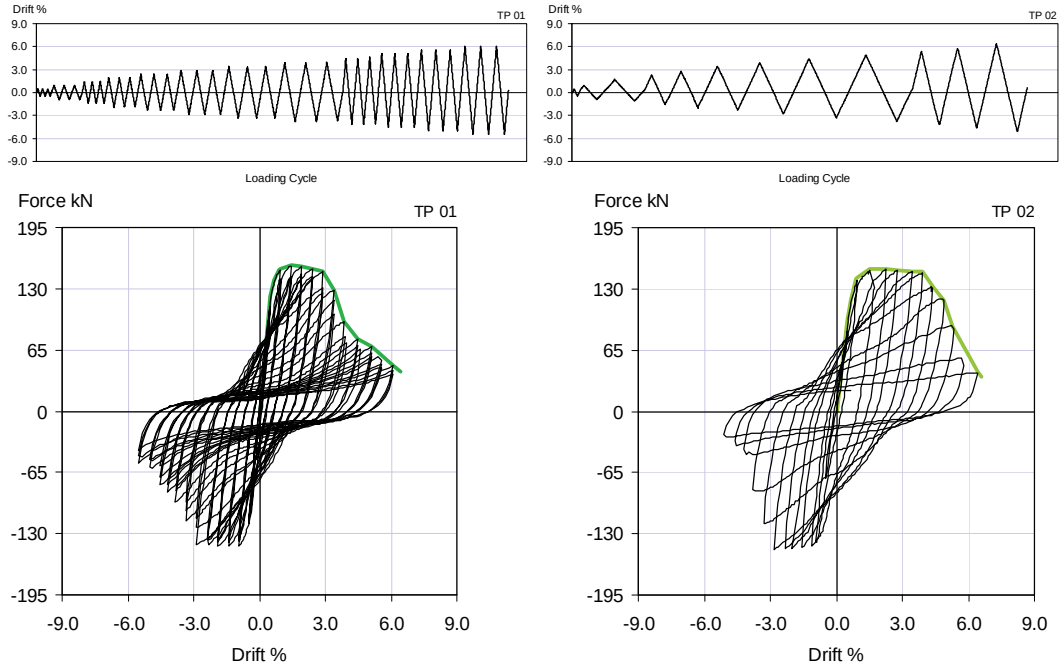

Figure 2-17 Loading protocols and resulting hysteretic plots for identical reinforced concrete bridge pier specimens: (a) Loading Protocol TP01; and (b) Loading Protocol TP02 (adapted from Takemura and Kawashima, 1997).

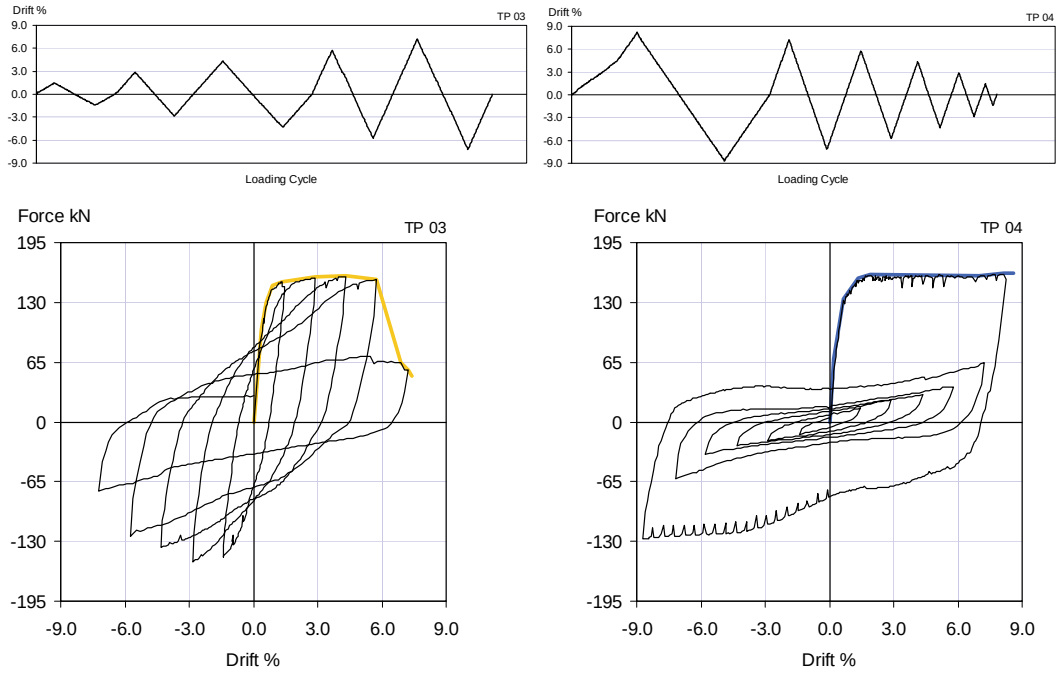

(a) (b)

Figure 2-18 Loading protocols and resulting hysteretic plots for identical reinforced concrete bridge pier specimens: (a) Loading Protocol TP03; and (b) Loading Protocol TP04 (adapted from Takemura and Kawashima, 1997).

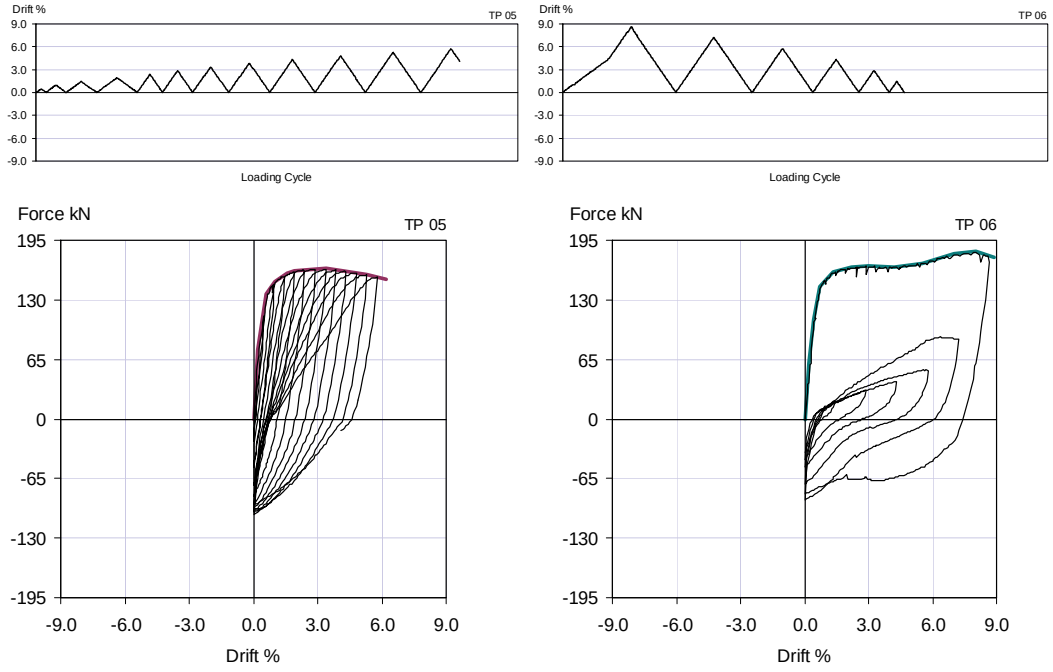

(a) (b)

Figure 2-19 Loading protocols and resulting hysteretic plots for identical reinforced concrete bridge pier specimens: (a) Loading Protocol TP05; and (b) Loading Protocol TP06 (adapted from Takemura and Kawashima, 1997).

The resulting cyclic envelopes are plotted together in Figure 2-20 for comparison. Loading protocols with more cycles and increasing amplitudes in each cycle (e.g., TP 01, TP 02, and TP 03) resulted in smaller cyclic envelopes. Loading protocols with fewer cycles and decreasing in amplitudes in each cycle (e.g., TP 04 and TP 06) resulted in larger cyclic envelopes.

These studies show that if nominally identical specimens are loaded with different loading protocols, their cyclic envelope will change depending on the number of cycles used in the loading protocol, the amplitude of each cycle, and the sequence of the loading cycles.

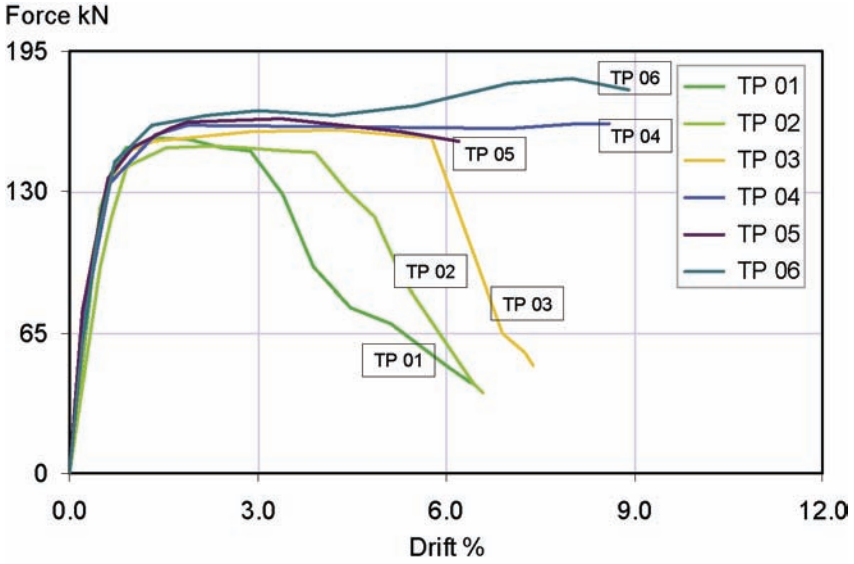

Figure 2-20 Comparison of cyclic envelopes of reinforced concrete bridge pier specimens subjected to six different loading protocols (adapted from Takemura and Kawashima, 1997).

2.2.4 Relationship between Loading Protocol, Cyclic Envelope, and Force-Displacement Capacity Boundary

For analytical purposes, a series of hysteretic rules can be specified to control the hysteretic behavior of a component within a force-displacement capacity boundary. Unless a loading protocol has forced the structural component or system to reach the force-displacement capacity boundary, the resulting cyclic envelope will be smaller, and in some cases significantly smaller, than the actual capacity boundary.

Figure 2-21 shows the cyclic envelope for a structural component subjected to a single loading protocol. In Figure 2-21a, the cyclic envelope is equal to the force-displacement capacity boundary. In Figure 2-21b, the force-displacement capacity boundary extends beyond the cyclic envelope (which

would be the case if the component actually had more force-displacement capacity than indicated by a single cyclic envelope).

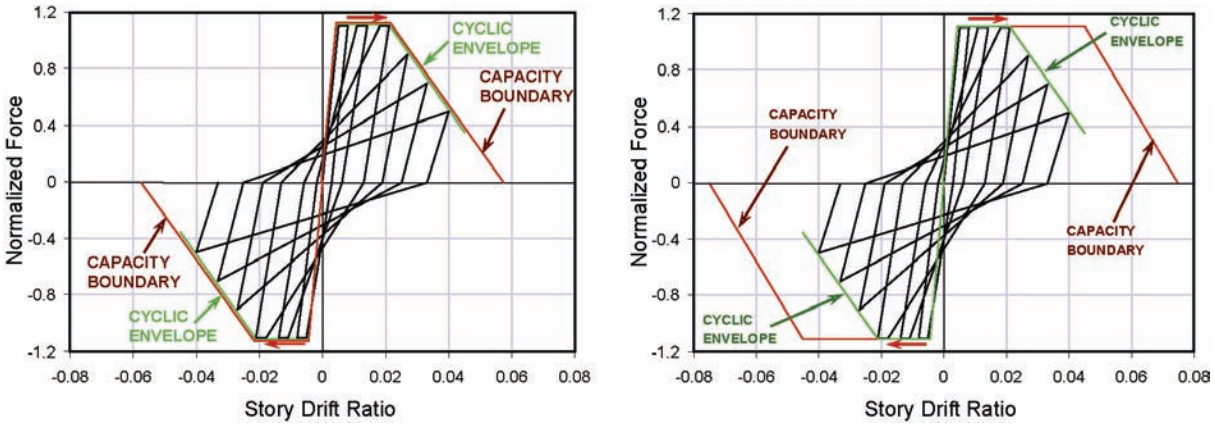

(a) (b)

Figure 2-21 Examples of a force-displacement capacity boundary that is (a) equal to the cyclic envelope, and (b) extends beyond the cyclic envelope.

Figure 2-22 shows the hysteretic behavior of the same component subjected to a different loading protocol. In this protocol the first four cycles are the same, but in the fifth cycle additional lateral displacement is imposed up to a peak story drift ratio of 5.5%. In Figure 2-22a, the component reaches the force-displacement capacity boundary and the response is forced to follow a downward slope along the boundary (in-cycle strength degradation). Eventually, zero lateral resistance is reached before the unloading cycle can begin.

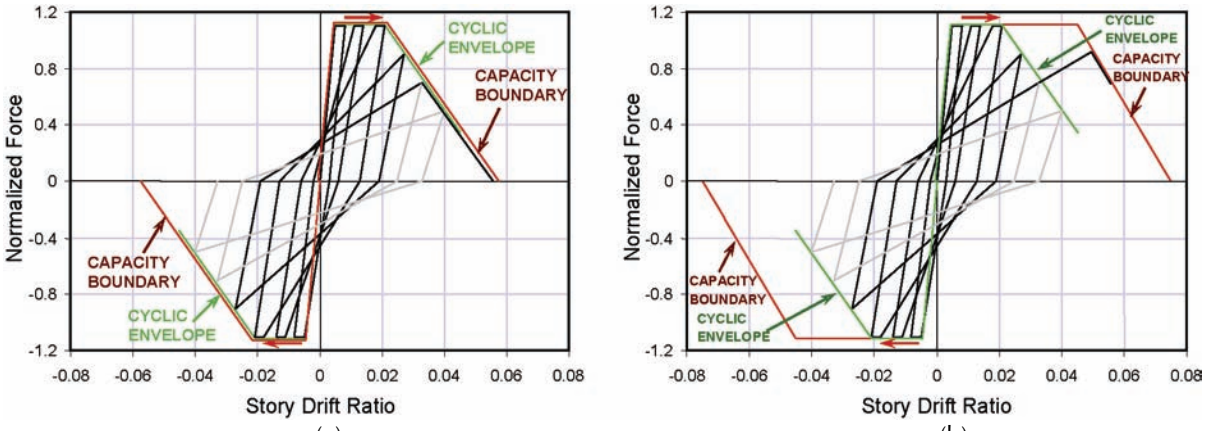

(a) (b)

Figure 2-22 Comparison of hysteretic behavior when the force-displacement capacity boundary is: (a) equal to the cyclic envelope, and (b) extends beyond the cyclic envelope.

In Figure 2-22b, however, because the force-displacement capacity boundary extends beyond the cyclic envelope, the component has additional capacity to resist deformation. As the lateral displacement approaches 5.5%, the

response continues to gain strength until the force-displacement capacity boundary is reached. The response is then forced to follow along the boundary (in-cycle strength degradation) until the unloading cycle commences at peak story drift ratio of 5.5%. In this case the component can continue to resist 70% of its peak lateral strength at a story drift ratio of 5.5%, rather than degrading to zero lateral resistance before unloading occurs.

Under lateral displacements that are less than or equal to those used to generate the cyclic envelope, differences between the cyclic envelope and the force-displacement capacity boundary are of no consequence. However, under larger lateral displacements these differences will affect the potential for in-cycle degradation to occur, which will significantly affect system behavior and response. Determining the force-displacement capacity boundary based on the results of a single cyclic loading protocol can result in overly conservative results due to significant underestimation of the actual force-displacement capacity and subsequent overestimation of lateral displacement demands.

Chapter 3
Development of Single-Degree-of-Freedom Models for Focused Analytical Studies

This chapter describes the development of single-degree-of-freedom models, and explains the analytical procedures used in the conduct of focused analytical studies.

3.1 Overview of Focused Analytical Studies

3.1.1 Purpose

From past research, it is apparent that in-cycle strength and stiffness degradation are real phenomena that have been observed and documented to cause instability in individual components. Little experimental information exists, however, on whether or not larger assemblies of components of mixed hysteretic behavior experience similar negative stiffness that could lead to dynamic instability. In order to further investigate the response of systems with degrading components, focused analytical studies were conducted. The purpose of these studies was to test and quantify the effects of different degrading behaviors on the dynamic stability of structural systems.

3.1.2 Process

Studies consisted of nonlinear dynamic analyses of single-degree-of-freedom oscillators with varying system characteristics. Characteristics under investigation included differences in hysteretic behavior, such as cyclic versus in-cycle degradation, and variations in the features of the force-displacement capacity boundary, such as the point at onset of degradation, the slope of degradation, the level of residual strength, length of the residual strength plateau, and ultimate deformation capacity (Figure 3-1).

The process used for developing, analyzing, and comparing structural system models in the focused analytical studies was as follows:

- A set of single-degree-of-freedom (SDOF) springs were developed featuring different hysteretic and force-displacement capacity boundary characteristics. While not an exact representation of the mechanical

behavior of any one specific structural component, springs were intended to capture the major characteristics of force-displacement capacity boundaries for systems that would typically be encountered in practice.

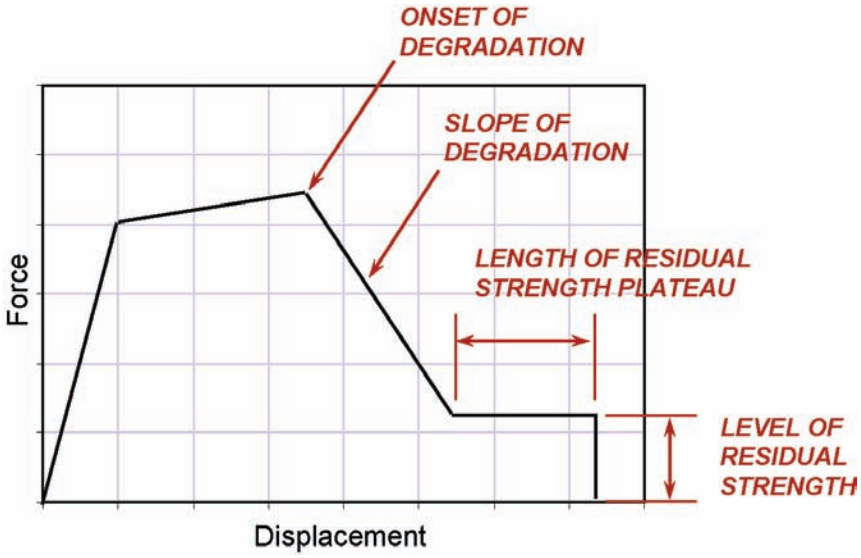

Figure 3-1 Features of the force-displacement capacity boundary varied in focused analytical studies.

- Multiple spring models were used to represent the behavior of more complex structural systems containing subsystems with different hysteretic and force-displacement capacity boundary characteristics. Multi-spring SDOF systems were developed by placing two individual springs in parallel, linked by a rigid diaphragm.
- Nonlinear response history analyses were performed using the Open System for Earthquake Engineering Simulation (OpenSEES) software (Fenves and McKenna, 2004). In OpenSEES, structural system models were subjected to the Incremental Dynamic Analysis (IDA) procedure (Vamvatsikos and Cornell, 2002) in which the nonlinear dynamic response of individual and multiple spring systems were evaluated at incrementally increasing levels of ground motion intensity.
- Results were compared in two ways: (1) among systems with different components that were tuned to have the same global yield strength and the same period of vibration; and (2) among systems composed of the same two components but having different relative contributions from each, thus exhibiting different strength and stiffness characteristics. Comparisons between systems tuned to the same yield strength and period of vibration were used to observe the influence of different hysteretic rules and force-displacement capacity boundary characteristics. Comparisons between systems composed of the same

components, but with different strength and stiffness characteristics, were used to observe the relative contribution from each subsystem on overall system response.

3.1.3 Incremental Dynamic Analysis Procedure

Focused analytical studies were conducted using the Incremental Dynamic Analysis (IDA) procedure (Vamvatsikos and Cornell, 2002). Incremental dynamic analysis is a type of response history analysis in which a system is subjected to ground motion records scaled to increasing levels of intensity until lateral dynamic instability is observed. In incremental dynamic analysis, intensity is characterized by a selected intensity measure (IM), and lateral dynamic instability occurs as a rapid, nearly infinite increase in the engineering demand parameter (EDP) of interest, given a small increment in ground motion intensity.

3.1.3.1 Intensity measures

Two intensity measures were used in conducting incremental dynamic analyses. One was taken as the 5% damped spectral acceleration at the fundamental period of vibration of the oscillator, $S_a(T,5\%)$. This measure is generally appropriate for single-degree-of-freedom systems. It, however, does not allow comparison among systems having different periods of vibration. For this reason, a normalized intensity measure, $R = S_a(T,5\%)/S_{ay}(T,5\%)$ was also used, where $S_{ay}(T,5\%)$ is the intensity that causes first yield to occur in the system. This places first yield at a normalized intensity of one.

The normalized intensity measure $S_a(T,5\%)/S_{ay}(T,5\%)$ closely resembles the strength ratio, R, which is a normalized strength that is often used in studies of SDOF systems (see Chapter 2). Higher values of the normalized intensity measure $S_a(T,5\%)/S_{ay}(T,5\%)$ represent systems with lower lateral strength. Note that the R-factor discussed here is not the same as the response-modification coefficient used in code-based equivalent lateral force design procedures. Rather, it is essentially the system ductility reduction factor, R_d, as defined in the *NEHRP Recommended Provisions for Seismic Regulations for New Buildings and Other Structures, Part 2: Commentary* (FEMA, 2004b).

3.1.3.2 Engineering Demand Parameters

The engineering demand parameter of interest was taken as story drift ratio. This parameter is a normalized measure of lateral displacement that allows for non-dimensional comparison of results. Lateral dynamic instability

occurs when solutions to the input ground motion fail to converge, implying infinite lateral displacements.

3.1.3.3 Collapse

Lateral dynamic instability is manifested in structural systems as sidesway collapse caused by loss of lateral-force-resisting capacity. Sidesway collapse mechanisms can be explicitly simulated in incremental dynamic analyses, and comparisons of analytical results are based on this limit state.

It should be noted, however, that behavior of real structures can include loss of vertical-load-carrying capacity at lateral displacements that are significantly smaller than those associated with sidesway collapse. Inelastic deformation of structural components can result in shear and flexural-shear failures in members, and failures in joints and connections, which can lead to an inability to support vertical loads (vertical collapse) long before sidesway collapse can be reached. Differences between sidesway and vertical collapse behaviors are shown in Figure 3-2.

(a) (b)

Figure 3-2 Different collapse behaviors: (a) vertical collapse due to loss of vertical-load-carrying capacity; and (b) incipient sidesway collapse due to loss of lateral-force-resisting capacity (reproduced with permission of EERI).

Consideration of vertical collapse modes is beyond the scope of this investigation, however, collapse simulation and explicit consideration of both vertical and sidesway collapse modes are described in FEMA P695 *Quantification of Building Seismic Performance Factors* (FEMA, 2009).

3.1.3.4 Incremental Dynamic Analysis Curves

By plotting discrete intensity measure/engineering demand parameter pairs in an IM-EDP plane, the results of incremental dynamic analyses can be

displayed as a suite of IDA curves, one curve corresponding to each ground motion record. An example of one such suite of curves is shown in Figure 3-3, where IDA curves computed from 30 different ground motions are shown. Curves in this figure are plotted with the normalized intensity measure $R = S_a/S_a^{yield}$ on the vertical axis, and normalized engineering demand parameter $\mu = \delta/\delta^{yield}$ on the horizontal axis.

The IDA curves in Figure 3-3a have a common characteristic in that they all terminate with a distinctive horizontal segment, referred to as "flatline." Horizontal segments in IDA curves mean that large displacements occur at small increments in ground motion intensity, which is indicative of lateral dynamic instability. The intensity (or normalized intensity) at which IDA curves become horizontal is taken as the sidesway collapse capacity of the system.

As shown in Figure 3-3a, the sidesway collapse capacity varies significantly from one ground motion record to another. This variability in response is known as record-to-record variability. Because of record-to-record variability, the response due to any one record is highly uncertain. For this reason, statistical information on response due to a suite of ground motions is used to quantify the central tendency (median) and variability (dispersion) of the behavior of a structural system.

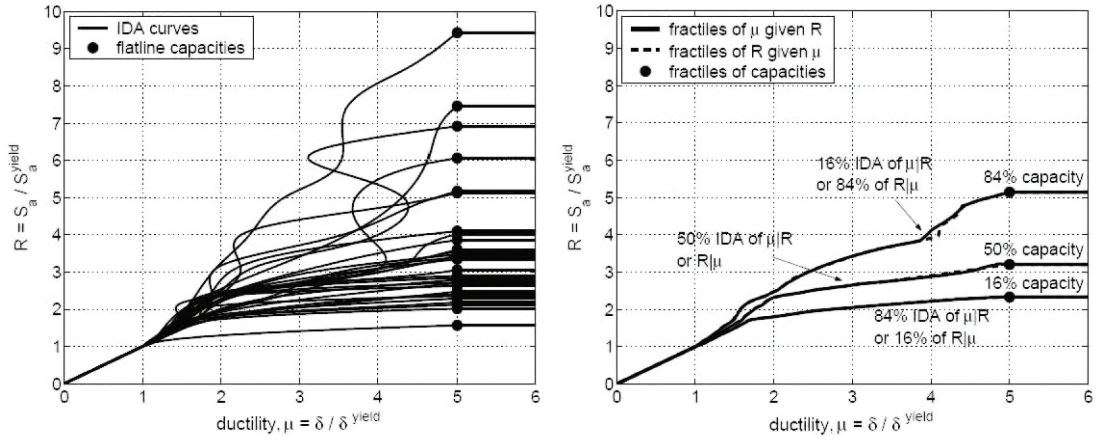

(a) Thirty IDA curves and flatline capacities (b) Summarization into fractile IDAs, given R or μ

Figure 3-3 Examples depicting incremental dynamic analysis results; (a) suite of individual IDA curves from 30 different ground motion records; and (b) statistically derived quantile curves given μ or R (Vamvatsikos and Cornell 2006)

Figure 3-3b shows quantiles (i.e., 16th, 50th (median) and 84th percentiles) of collapse capacity derived from the results of the 30 IDA curves shown in Figure 3-3a. Also shown in Figure 3-3b, are the 16th, 50th (median) and 84th percentile curves of normalized deformation demands for given normalized

ground motion intensities (μ given R), and normalized ground motion intensities for given lateral deformation demands (R given μ). In the figure, the median curve for μ given R is approximately the same as the median curve for R given μ; the 16th percentile curve for μ given R is approximately the same as the 84th percentile curve for R given μ; and the 84th percentile curve for μ given R is approximately the same as the 16th percentile curve for R given μ.

Computing normalized ground motion intensities for given lateral deformation demands (i.e., R given μ) is an iterative process (Ruiz-Garcia and Miranda, 2003). Further complicating this process is that, in certain cases, there can be multiple intensity levels corresponding to a given lateral deformation demand (Vamvatsikos and Cornell, 2002). For these reasons, results in this investigation are reported using quantiles of lateral deformation demand given ground motion intensity (i.e., μ given R).

Use of quantiles of deformation given intensity (i.e., μ given R) means that 16% of the lateral deformation demands for a given level of ground motion intensity would be to the left of the 16th percentile IDA curve, and that 84% would be to the right. Thus, the 16th percentile IDA curve for μ given R will always be above the median curve. Similarly, the 84th percentile IDA curve for μ given R will always be below the median curve.

3.1.4 Ground Motion Records

Analyses were performed using an early version of the ground motion record set selected for use in the ATC-63 Project, and provided in FEMA P695 *Quantification of Building Seismic Performance Factors* (FEMA, 2009). In general this set is intended to include far-field records from all large-magnitude events in the PEER NGA database (PEER, 2006). To avoid event bias, no more than two records were taken from any one earthquake.

In total 28 sets of two horizontal components were used (see Table 3-1). This record set is similar, but not identical, to the set ultimately selected for use in FEMA P695. All records are from firm soil sites, and none include any traces of near source directivity. Values of peak ground acceleration (PGA) and peak ground velocity (PGV) shown in the table correspond to the largest of the two horizontal components.

Table 3-1 Earthquake Records Used in Focused Analytical Studies (Both Horizontal Components)

Event[1] Station	R [2] Km	Vs30 [3] m/s	φ_1 [4] Deg	φ_2 [4] deg	PGA g	PGV cm/s
Northridge 1994 (M=6.7)						
1. Beverly Hills, Mullholland Dr.	9.4	356	009	279	0.52	57.2
2. Canyon Country, W Lost Canyon	11.4	309	000	270	0.48	44.8
Kern County 1952 (M=7.4)						
3. Taft Lincoln School	38.4	385	021	111	0.18	15.6
Borrego Mtn 1968 (M=6.6)						
4. El Centro Array #9	45.1	213	180	270	0.13	18.5
Duzce Turkey 1999 (M=7.1)						
5. Bolu	12	326	000	090	0.82	59.2
Hector Mine 1999 (M=7.1)						
6. Armboy	41.8	271	090	360	0.18	23.2
7. Hector	10.4	685	000	090	0.34	34.1
Imperial Valley 1979 (M=6.5)						
8. Delta	22	275	262	352	0.35	28.4
9. El centro Array #11	12.5	196	140	230	0.38	36.7
Kobe, Japan 1995 (M=6.9)						
10. Nishi-Akashi	7.1	609	000	090	0.51	36.1
11. Shin-Osaka	19.1	256	000	090	0.24	33.9
Kocaeli, Turkey 1999 (M=7.5)						
12. Duzce	13.6	276	180	270	0.36	54.1
13. Arcelik	10.6	523	000	090	0.22	27.4
Landers 1992 (M=7.3)						
14. Yermo Fire Station	23.6	354	270	360	0.24	37.7
15. Coolwater	19.7	271	long	trans	0.42	32.4
Loma Prieta 1989 (M=6.9)						
16. Capitola	8.7	289	000	090	0.53	34.2
17. Gilroy Array #3	12.2	350	000	090	0.56	42.3
Manjil Iran 1990 (M=7.4)						
18. Abbar	12.6	724	long	trans	0.51	47.3

Table 3-1 Earthquake Records Used in Focused Analytical Studies (Both Horizontal Components) *(continued)*

Event[1] Station	R [2] Km	Vs30 [3] m/s	φ_1 [4] Deg	φ_2 [4] deg	PGA g	PGV cm/s
Superstition Hills 1987 (M=6.7)						
19. El Centro Imp. Co Cent	18.2	192	000	090	0.36	42.8
20. Poe Road	11.2	208	270	360	0.45	31.7
Cape Mendocino 1992 (M=7.0)						
21. Eureka – Myrtle and West	40.2	339	000	090	0.18	24.2
22. Rio Dell Overpass – FF	7.9	312	270	360	0.55	45.4
Chi-Chi, Taiwan 1999 (M=7.6)						
23. CHY101	10.0	259	090	000	0.44	90.7
24. TCU045	26.0	705	090	000	0.51	38.8
San Fernando, 1971 (M=6.6)						
25. LA Hollywood Sto FF	22.8	316	090	180	0.21	17.8
St Elias, Alaska 1979 (M=7.5)						
26. Yakutat	80.0	275	009	279	0.08	34.3
27. Icy Bay	26.5	275	090	180	0.18	26.6
Friuli, Italy 1976 (M=6.5)						
28. Tolmezzo	15.0	425	000	270	0.35	25.9

[1] Moment magnitude
[2] Closest distance to surface projection of fault rupture
[3] S-wave speed in upper 30m of soil
[4] Component

3.1.5 Analytical Models

The basis of the focused analytical studies is a set of idealized spring models representative of the hysteretic and force-displacement capacity boundary characteristics of different structural systems. The springs were modeled using the Pinching4, ElasticPP and MinMax uniaxial materials in OpenSEES. The Pinching4 material allows the definition of a complex multi-linear force-displacement capacity boundary composed of four linear segments. The ElasticPP material defines a system with an elasto-plastic force-displacement capacity boundary. The MinMax material allows the setting of an ultimate drift at which a system loses all its lateral-force-resisting capacity in both loading directions. The Pinching4 and ElasticPP materials in combination with MinMax were used to define springs with the

desired force-displacement capacity boundary characteristics along with finite ultimate deformation capacities.

Parametric studies were conducted on single-degree-of-freedom (SDOF) oscillators constructed with these springs and their variants. Generic story-models were developed using single-spring systems or multi-spring systems consisting of two springs in parallel. Story models were intended to approximate the behavior of single-story systems composed of an individual subassembly or a mixture of subassemblies having complex hysteretic and force-displacement capacity boundary characteristics linked by rigid diaphragms.

3.2 Single-Spring Models

Each single-spring system model is defined by a hysteretic model confined within a force-displacement boundary (Figure 3-4) developed from information available in the literature. The single-spring systems are based on the following set of eight different hysteretic behaviors and force-displacement capacity boundary characteristics:

- Spring 1 – typical gravity frame system (e.g., steel)
- Spring 2 – non-ductile moment frame system (e.g., steel or concrete)
- Spring 3 – ductile moment frame system (e.g., steel or concrete)
- Spring 4 – stiff non-ductile system (e.g., steel concentric braced frame)
- Spring 5 – stiff, highly-pinched non-ductile system (e.g., brittle infill wall)
- Spring 6 – elastic-perfectly-plastic system (for comparison)
- Spring 7 – limited-ductility moment frame system (e.g., concrete)
- Spring 8 – non-ductile gravity frame system (e.g., concrete)

While intended to be representative of realistic degrading response that has been observed to occur in some structural components, these idealized springs are not intended to be a detailed characterization of the mechanical behavior of any one specific structural component or structural subassembly. Rather, they are used to capture the main response characteristics of components or subassemblies that are often present and combined in real structural systems. The focus was not on investigating the seismic performance of a particular structural system, but on identifying the effects of various aspects of degrading behavior on the response of one-story single-degree-of-freedom system models.

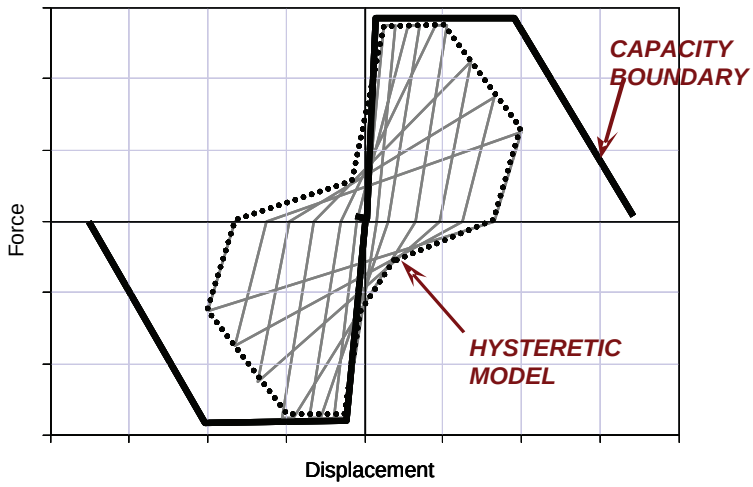

Figure 3-4 Hysteretic model confined by a force-displacement capacity boundary.

An “a” and “b” version of each spring was developed. The “a” and “b” versions differ by one or two characteristics of the force-displacement capacity boundary so that the “b” version always possesses the more favorable characteristics of the two. Sources of variation included the point at onset of degradation, the slope of degradation, the level of residual strength, and length of the residual strength plateau. To investigate period dependency, systems utilizing the “a” and “b” versions of each individual spring were tuned to periods of 0.5s, 1.0s, 1.5s, 2.0s, and 2.5s.

All springs were defined to be symmetrical, using the same force-displacement capacity boundary in both the positive and negative loading directions. All have a finite ultimate deformation capacity at which all lateral-force-resisting capacity is lost, and all, except for Spring 6 (which is elastic-perfectly-plastic), include in-cycle strength degradation.

In addition, the “a” and “b” versions of each spring (except for Spring 6) were analyzed with both a constant force-displacement capacity boundary and a degrading force-displacement capacity boundary in order to quantify the effect of cyclic degradation on system response. To do this, springs were subjected to an ATC-24 type loading protocol (ATC, 1992), consisting of two cycles at each level of drift starting at 0.5% drift, and increasing in increments of 1% drift up to a maximum of 8% drift.

The generic force-displacement capacity boundary used for all springs is shown in Figure 3-5. The values of normalized base shear, F/F_y, and story drift ratio, θ, chosen to characterize the force-displacement capacity boundary for each of the single-spring system models are listed in Table 3-2.

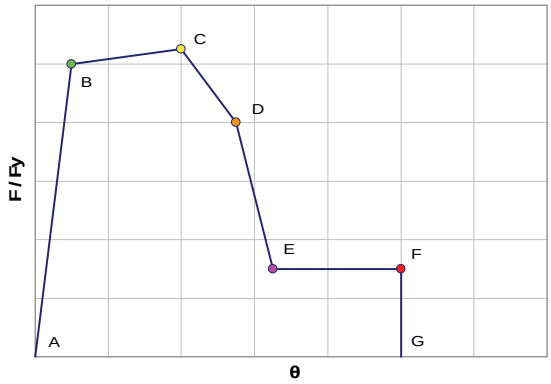

Figure 3-5 Generic force-displacement capacity boundary used for all single-spring system models.

For purposes of comparison, one version of each spring is shown in Figure 3-6. The parameters that define each spring, and the variations in each spring, are described in more detail in the sections that follow.

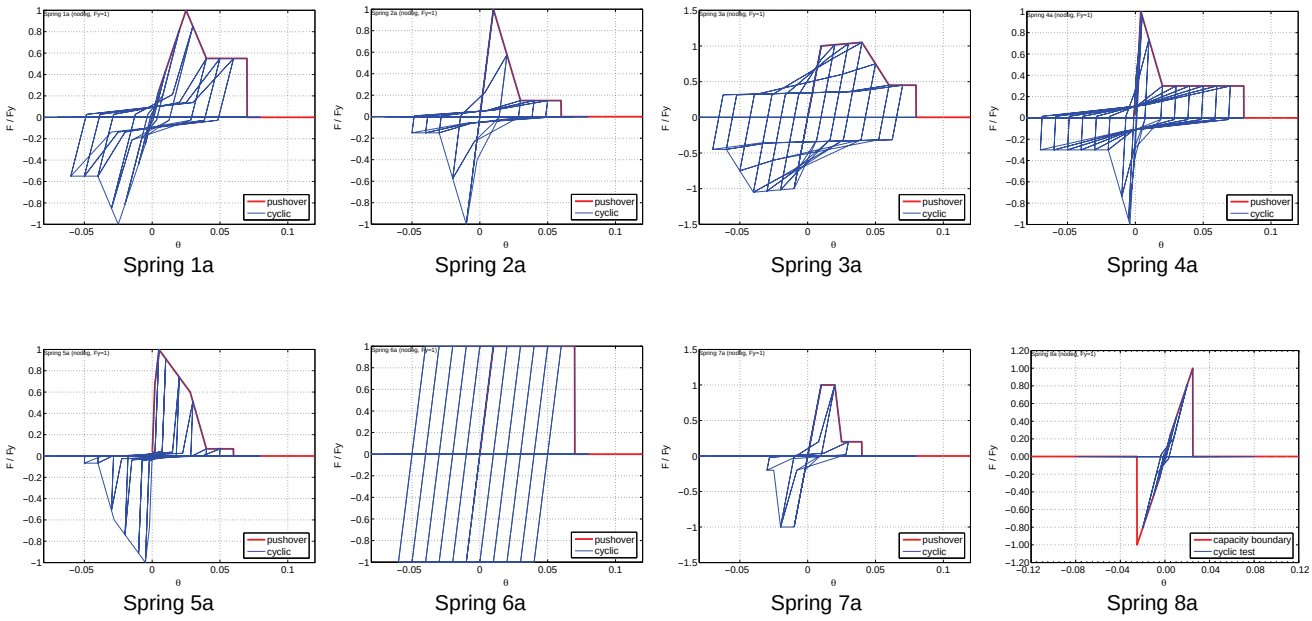

Figure 3-6 Comparison of eight basic single-spring system models.

Table 3-2 Force-Displacement Capacity Boundary Control Points for Single-Spring System Models.

Prototype	Type	Quantity	Points of the force-deformation capacity boundary						
			A	B	C	D	E	F	G
Typical gravity frame	1a	F/Fy	0	0.25	1	0.55	0.55	0.55	0
		θ	0	0.005	0.025	0.04	0.07	0.07	0.07
	1b	F/Fy	0	0.25	1	0.55	0.55	0.55	0
		θ	0	0.005	0.025	0.04	0.12	0.12	0.12
Non-ductile moment frame	2a	F/Fy	0	1	0.15	0.15	0.15	0.15	0
		θ	0	0.01	0.03	0.05	0.06	0.06	0.06
	2b	F/Fy	0	1	0.15	0.15	0.15	0.15	0
		θ	0	0.01	0.05	0.055	0.06	0.06	0.06
Ductile moment frame	3a	F/Fy	0	1	1.05	0.45	0.45	0.45	0
		θ	0	0.01	0.04	0.06	0.08	0.08	0.08
	3b	F/Fy	0	1	1.05	0.8	0.8	0.8	0
		θ	0	0.01	0.04	0.06	0.08	0.08	0.08
Stiff non-ductile system	4a	F/Fy	0	1	0.3	0.3	0.3	0.3	0
		θ	0	0.004	0.02	0.06	0.08	0.08	0.08
	4b	F/Fy	0	1	0.5	0.5	0.5	0.5	0
		θ	0	0.004	0.04	0.06	0.08	0.08	0.08
Stiff, highly pinched non-ductile system	5a	F/Fy	0	0.67	1	0.6	0.067	0.067	0
		θ	0	0.002	0.005	0.028	0.04	0.06	0.06
	5b	F/Fy	0	0.67	1	0.6	0.067	0.067	0
		θ	0	0.002	0.005	0.042	0.06	0.06	0.06
Elastic-perfectly-plastic	6a	F/Fy	0	1	1	1	1	1	0
		θ	0	0.01	0.02	0.03	0.07	0.07	0.07
	6b	F/Fy	0	1	1	1	1	1	0
		θ	0	0.01	0.02	0.03	0.12	0.12	0.12
Limited-ductile moment frame	7a	F/Fy	0	1	1	0.2	0.2	0.2	0
		θ	0	0.01	0.02	0.025	0.04	0.04	0.04
	7b	F/Fy	0	1	1	0.2	0.2	0.2	0
		θ	0	0.01	0.02	0.04	0.06	0.06	0.06
Non-ductile gravity frame	8a	F/Fy	0	1	1	0	0	0	0
		θ	0	0.025	0.025	0.025	0.025	0.025	0.025
	8b	F/Fy	0	1	1	0.55	0.55	0.55	0
		θ	0	0.025	0.025	0.03	0.04	0.04	0.04

3.2.1 *Springs 1a and 1b – Typical Gravity Frame Systems*

Springs 1a and 1b are intended to model the behavior of typical gravity frame systems in buildings. The force-displacement capacity boundary includes a strength drop immediately after yielding that terminates on a plateau with a residual strength of 55% of the yield strength (Figure 3-7). The "a" and "b" versions of this spring differ in the length of the residual strength plateau, which extends to an ultimate deformation capacity of 7% drift in Spring 1a and 12% drift in Spring 1b. This represents the maximum ductility that is achieved by any of the spring subsystems.

The hysteretic behaviors of Spring 1a and Spring 1b, both with and without cyclic degradation, are shown in Figure 3-8 and Figure 3-9. In each figure, the initial force-displacement capacity boundary (before cyclic degradation) is overlaid onto the hysteretic plots.

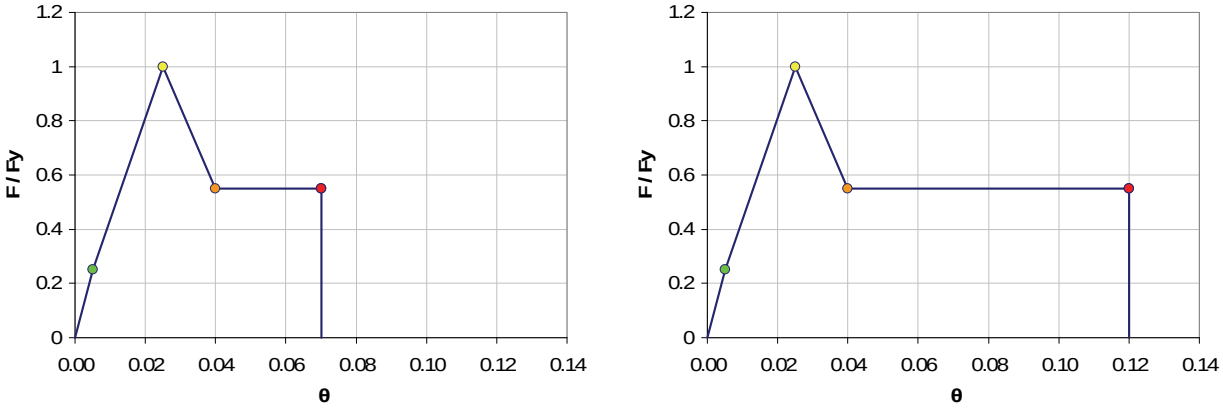

(Spring 1a) (Spring 1b)

Figure 3-7 Force-displacement capacity boundaries for Spring 1a and Spring 1b.

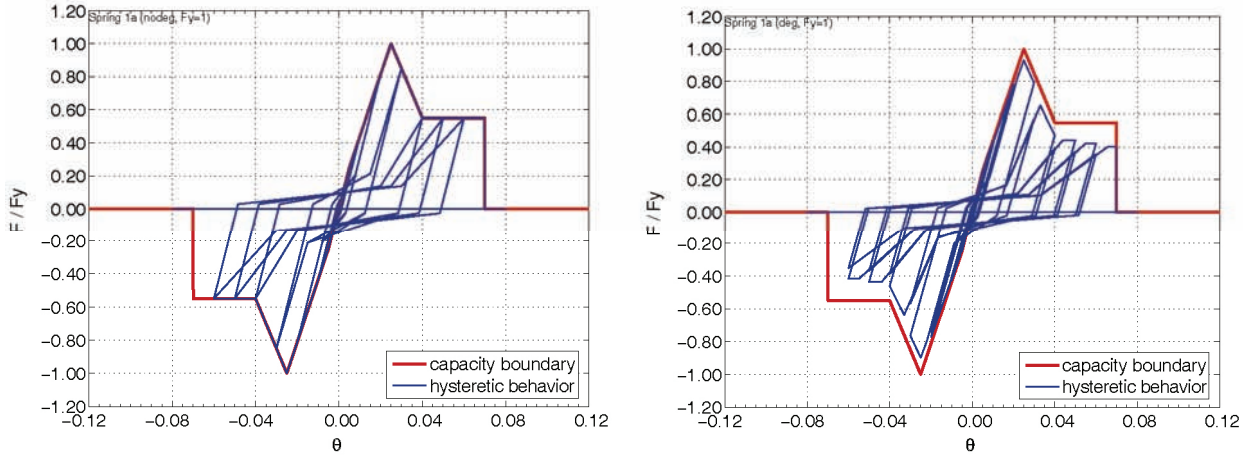

(a) (b)

Figure 3-8 Initial force-displacement capacity boundary overlaid onto hysteretic behaviors for Spring 1a: (a) without cyclic degradation; and (b) with cyclic degradation.

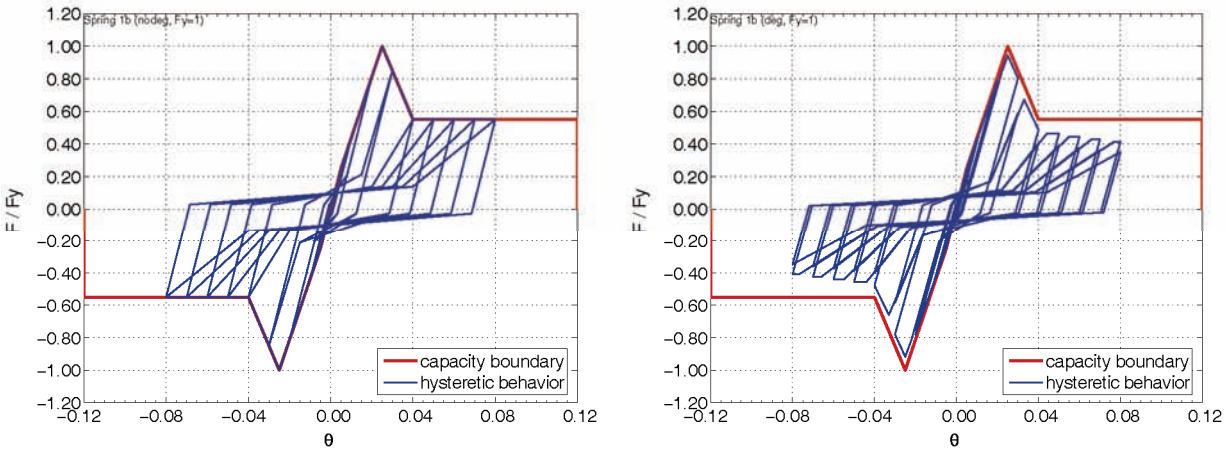

Figure 3-9 Initial force-displacement capacity boundary overlaid onto hysteretic behaviors for Spring 1b: (a) without cyclic degradation; and (b) with cyclic degradation.

Springs 1a and 1b are consistent with steel gravity frame systems with classic simple shear-tab connections. Experiments have shown that the gap between the beam and column flange is a critical parameter in determining force-displacement behavior of these systems. When a joint achieves enough rotation to result in contact between the beam and column flanges, bolts in the shear tab will be subjected to bearing strength failure, and the shear connection fails (Liu and Astaneh, 2003). This limit state marks the end of the residual strength plateau.

Spring 1a is consistent with a system in which beam/column flange contact occurs relatively early (7% drift), while Spring 1b is consistent with a system in which this contact occurs later (12% drift). Results from experimental tests on steel shear tab connections (Figure 3-10) exhibit a behavior that is similar to behavior the modeled in Springs 1a and 1b.

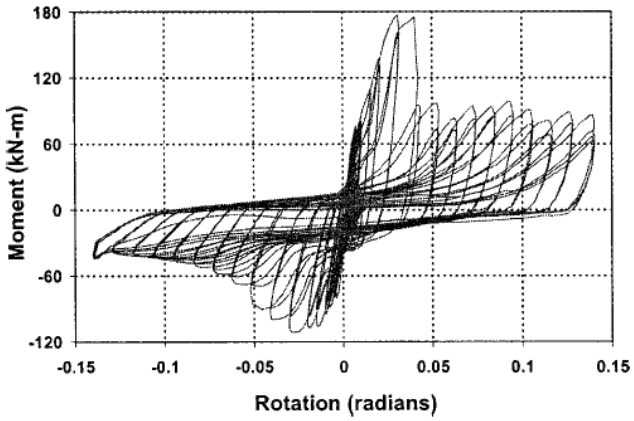

Figure 3-10 Hysteretic behavior from experimental tests on beam-to-column shear tab connections (Liu and Astaneh, 2003).

3.2.2 *Springs 2a and 2b – Non-Ductile Moment Frame Systems*

Springs 2a and 2b are intended to model the behavior of non-ductile moment-resisting frame systems in buildings. They are characterized by a force-displacement capacity boundary that includes strength degradation immediately after yielding, a low residual strength plateau at 15% of the yield strength, and an ultimate deformation capacity of 6% drift (Figure 3-11). The "a" and "b" versions of this spring differ in the negative slope of the strength-degrading segment, which is negative 43% in Spring 2a and negative 21% in Spring 2b.

The hysteretic behaviors of Spring 2a and Spring 2b, both with and without cyclic degradation, are shown in Figure 3-12 and Figure 3-13. In each figure, the initial force-displacement capacity boundary (before cyclic degradation) is overlaid onto the hysteretic plots.

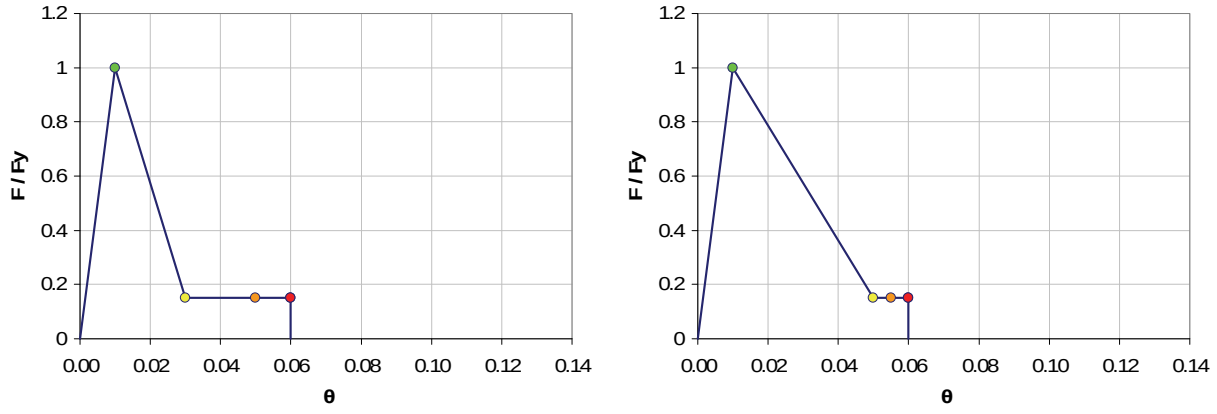

(Spring 2a) (Spring 2b)

Figure 3-11 Force-displacement capacity boundaries for Spring 2a and Spring 2b.

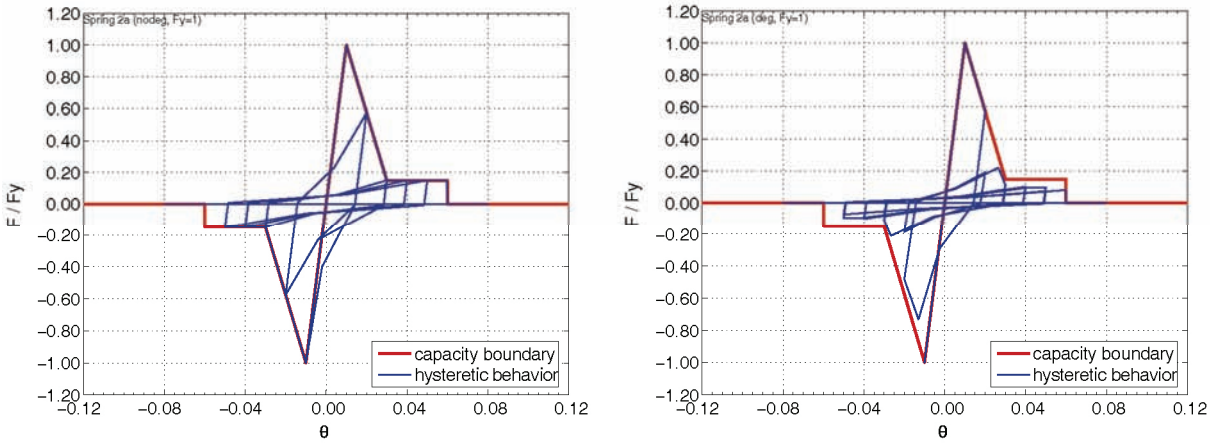

(a) (b)

Figure 3-12 Initial force-displacement capacity boundary overlaid onto hysteretic behaviors for Spring 2a: (a) without cyclic degradation; and (b) with cyclic degradation.

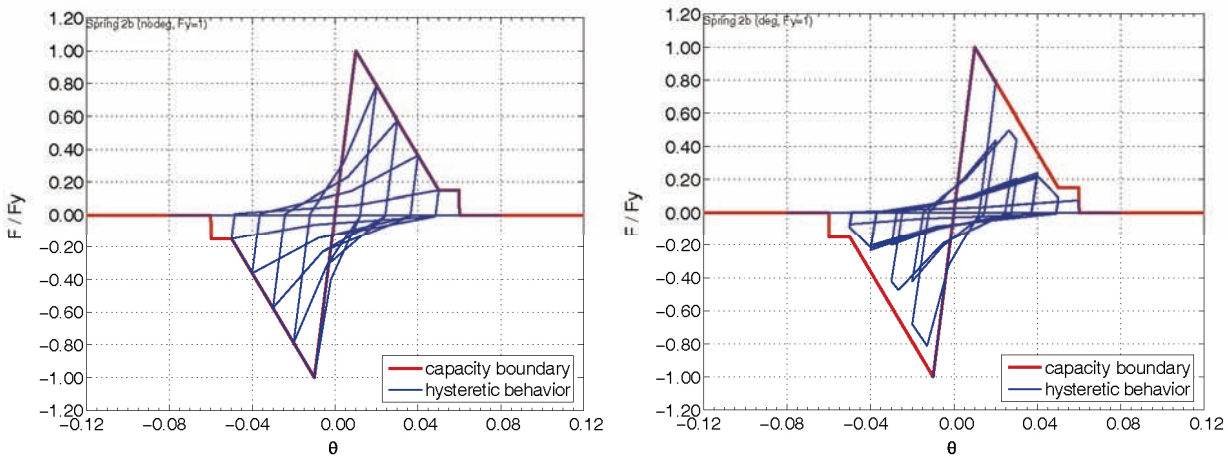

(a) (b)

Figure 3-13 Initial force-displacement capacity boundary overlaid onto hysteretic behaviors for Spring 2b: (a) without cyclic degradation; and (b) with cyclic degradation.

Systems with this behavior could be constructed in either steel or concrete. In the case of steel, these springs would be representative of moment-resisting frames with pre-Northridge welded beam-column connections, in which connection behavior is characterized by fracture and a large reduction in lateral force resistance. In the case of concrete, these springs would be representative of older (pre-1975) concrete frames with inadequate joint reinforcement, minimal concrete confinement and other poor detailing characteristics that would be prone to shear failure. Results from experimental tests on pre-Northridge welded steel connections and shear-critical reinforced concrete columns (Figure 3-14) exhibit a behavior that is similar to the behavior modeled in Springs 2a and 2b.

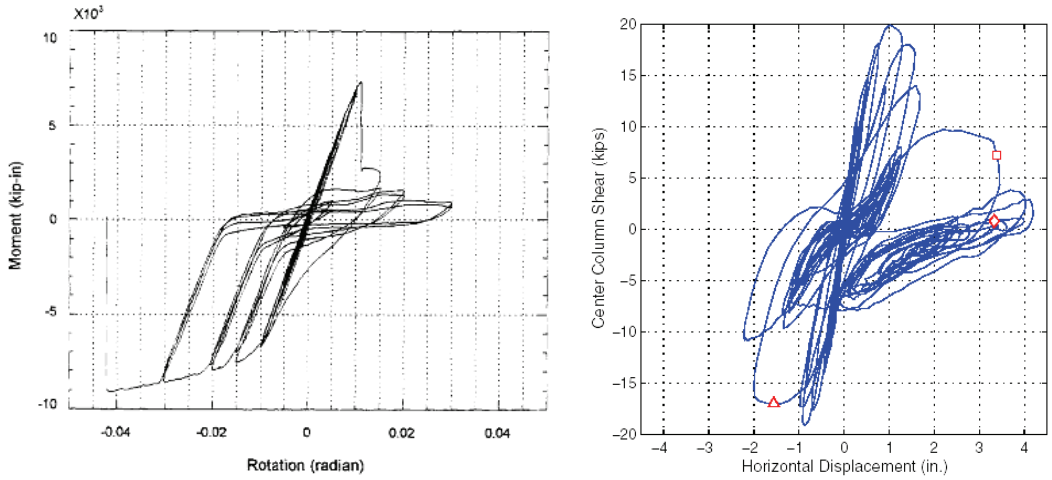

(a) (b)

Figure 3-14 Hysteretic behavior from experimental tests on: (a) pre-Northridge welded steel beam-column connections (Goel and Stojadinovic, 1999); and (b) shear-critical reinforced concrete columns (Elwood and Moehle, 2003).

3.2.3 *Springs 3a and 3b – Ductile Moment Frame Systems*

Springs 3a and 3b are intended to model the behavior of moderately-ductile moment-resisting frame systems in buildings. They are characterized by a force-displacement capacity boundary that includes a strength-hardening segment with a positive slope equal to 2% of the elastic stiffness, a strength-degrading segment that begins at 4% drift and ends at 6% drift, and a residual strength plateau with an ultimate deformation capacity of 8% drift (Figure 3-15). The "a" and "b" versions of this spring differ in the negative slope of the strength-degrading segment, which is negative 30% in Spring 3a and negative 13% in Spring 3b, and in the height of the residual strength plateau, which is 50% of yield in Spring 3a and 80% in Spring 3b.

The hysteretic behaviors of Spring 3a and Spring 3b, both with and without cyclic degradation, are shown in Figure 3-16 and Figure 3-17. In each figure, the initial force-displacement capacity boundary (before cyclic degradation) is overlaid onto the hysteretic plots.

Systems with this type of behavior could include special steel moment-resisting frames with ductile (e.g., post-Northridge) beam-column connections, or well-detailed reinforced concrete moment-resisting frames. Results from experimental tests on post-Northridge reduced beam steel moment connections (Figure 3-18) exhibit a behavior that is similar to the behavior modeled in Springs 3a and 3b.

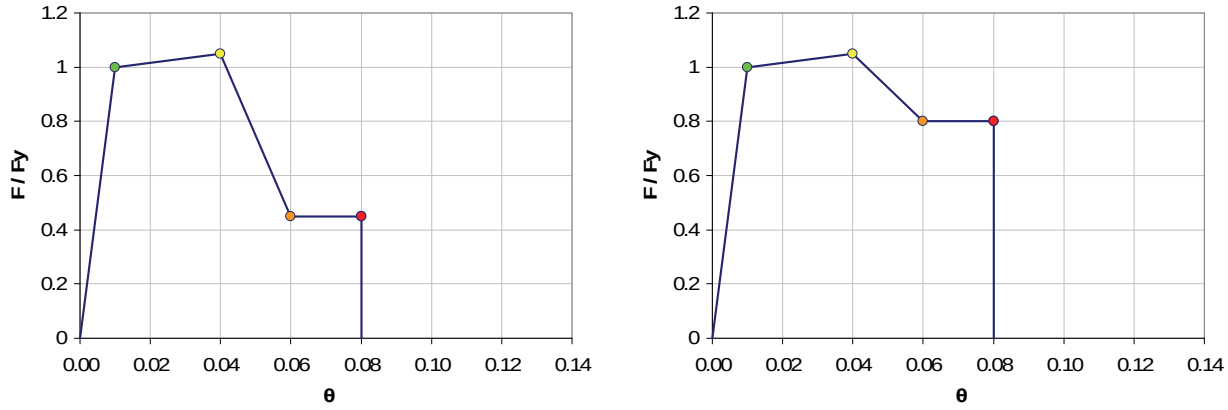

Figure 3-15 Force-displacement capacity boundaries for Spring 3a and Spring 3b.

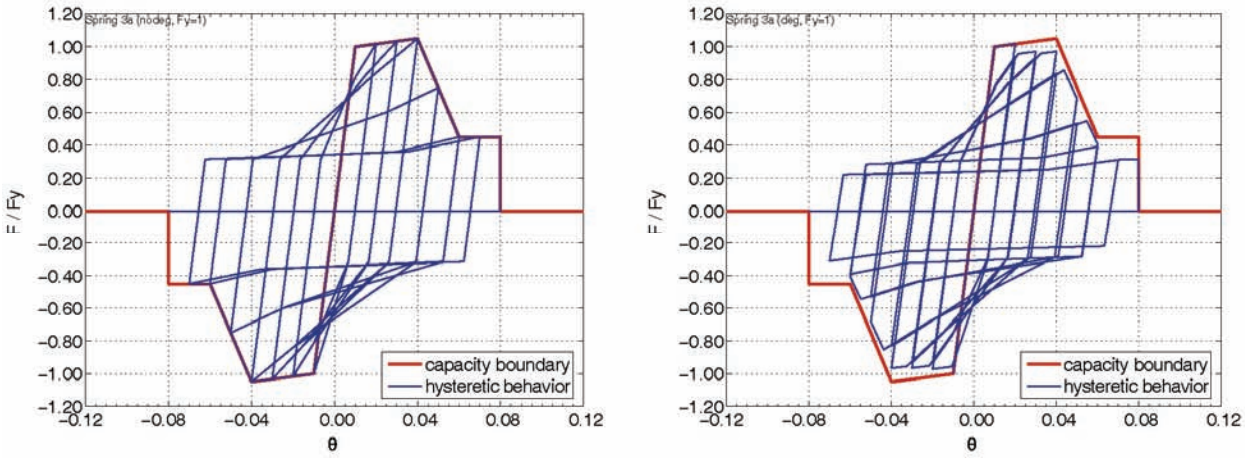

(a) (b)

Figure 3-16 Initial force-displacement capacity boundary overlaid onto hysteretic behaviors for Spring 3a: (a) without cyclic degradation; and (b) with cyclic degradation.

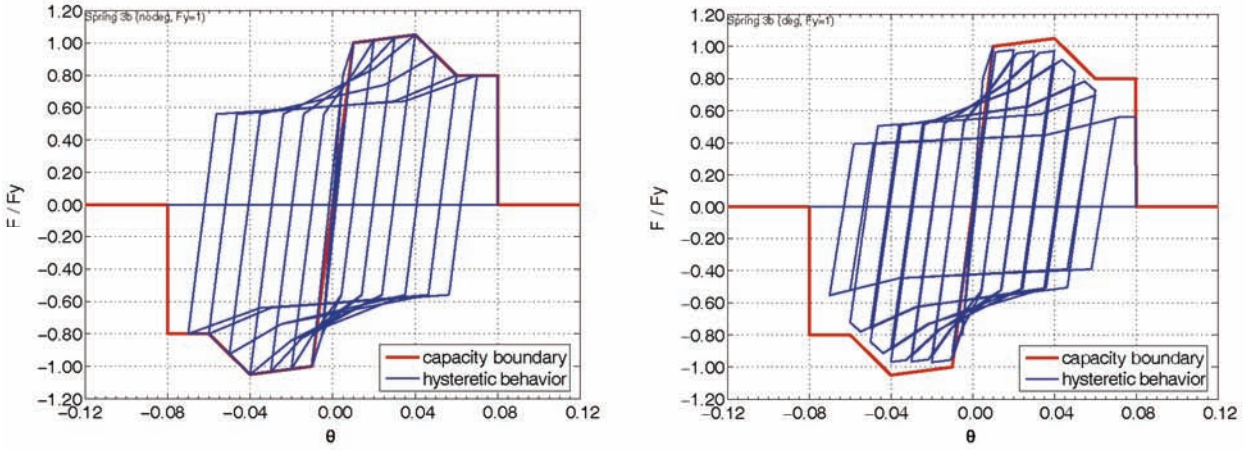

(a) (b)

Figure 3-17 Initial force-displacement capacity boundary overlaid onto hysteretic behaviors for Spring 3b: (a) without cyclic degradation and (b) with cyclic degradation.

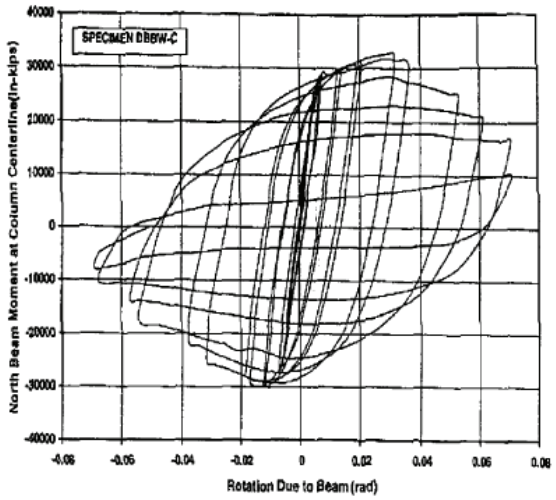

Figure 3-18 Hysteretic behavior from experimental tests on post-Northridge reduced-beam steel moment connections (Venti and Engelhardt, 1999).

3.2.4 *Springs 4a and 4b – Stiff, Non-Ductile Systems*

Springs 4a and 4b are intended to model the behavior of relatively stiff lateral-force-resisting systems that are subject to significant in-cycle strength degradation at small levels of deformation. They are characterized by a force-displacement capacity boundary that includes a strength-degrading segment beginning at 0.4% drift and terminating on a residual strength plateau with an ultimate deformation capacity of 8% drift (Figure 3-19). The "a" and "b" versions of this spring differ in the negative slope of the strength-degrading segment, which is negative 18% in Spring 4a and negative 6% in Spring 4b, and in the height of the residual strength plateau, which is 30% of yield in Spring 4a and 50% in Spring 4b.

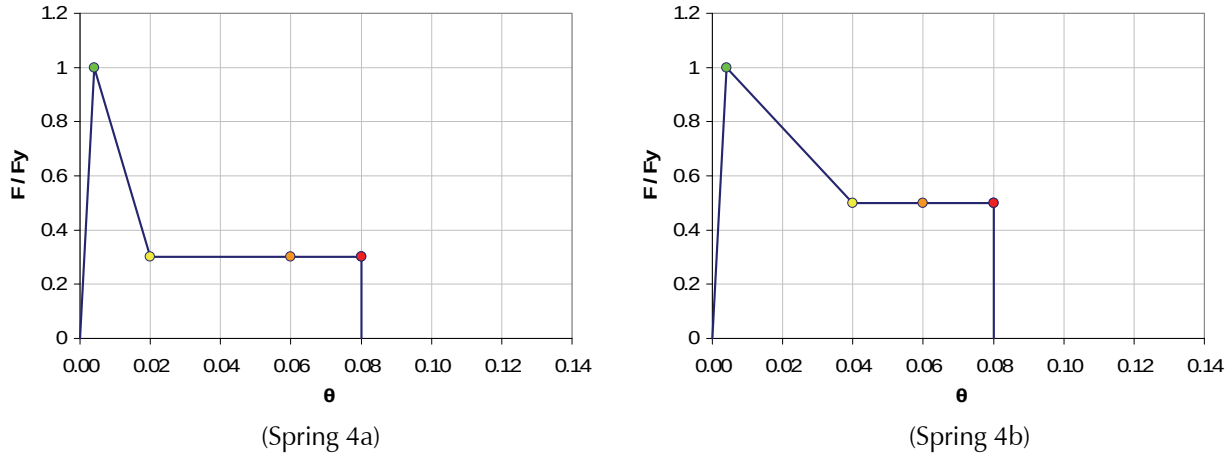

Figure 3-19 Force-displacement capacity boundaries for Spring 4a and Spring 4b.

The hysteretic behaviors of Spring 4a and Spring 4b, both with and without cyclic degradation, are shown in Figure 3-20 and Figure 3-21. They resemble a typical peak-oriented model with severe cyclic degradation of strength, unloading, and reloading stiffness parameters. In each figure, the initial force-displacement capacity boundary (before cyclic degradation) is overlaid onto the hysteretic plots.

Systems with this type of behavior could include steel concentric braced frames, which experience a sharp drop in strength following buckling of the braces at small levels of lateral deformation demand. Results from experimental tests on steel concentric braced frames (Figure 3-22) exhibit a behavior that is similar to the behavior modeled in Springs 4a and 4b.

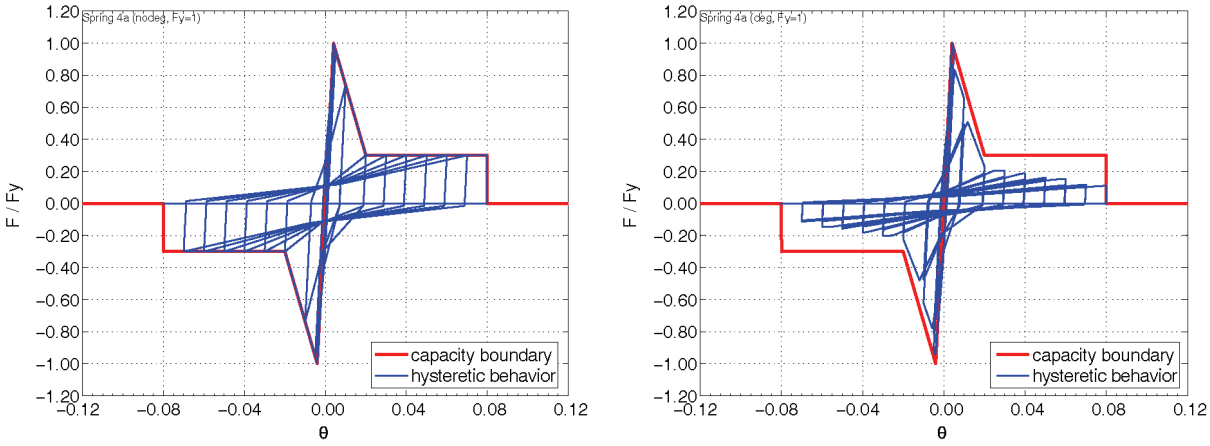

(a) (b)

Figure 3-20 Initial force-displacement capacity boundary overlaid onto hysteretic behaviors for Spring 4a: (a) without cyclic degradation; and (b) with cyclic degradation.

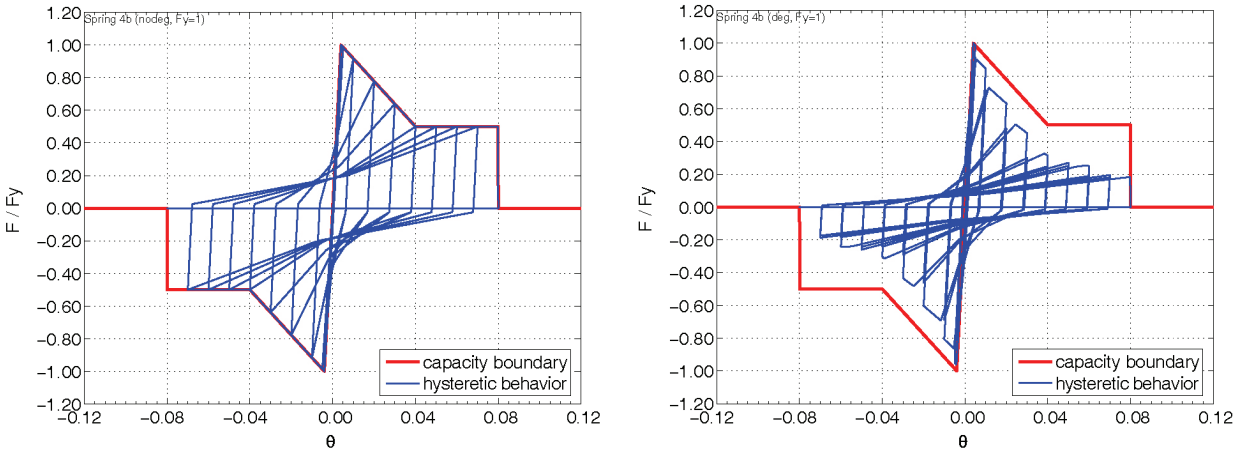

(a) (b)

Figure 3-21 Initial force-displacement capacity boundary overlaid onto hysteretic behaviors for Spring 4b: (a) without cyclic degradation; and (b) with cyclic degradation.

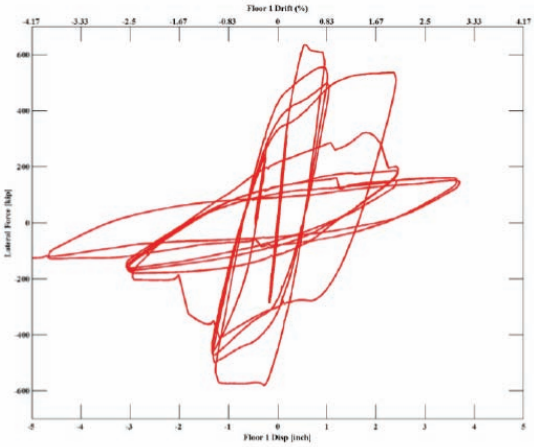

Figure 3-22 Hysteretic behavior from experimental tests on steel concentric braced frames (Uriz and Mahin, 2004).

3.2.5 *Springs 5a and 5b – Stiff, Highly-Pinched Non-Ductile Systems*

Springs 5a and 5b are intended to model the behavior of stiff and highly-pinched non-ductile lateral-force-resisting systems in buildings. They are characterized by a force-displacement capacity boundary with the highest initial stiffness of any of the spring subsystems, followed by varying levels of strength degradation and an ultimate deformation capacity of 6% drift (Figure 3-23). In both the "a" and "b" versions of this spring, peak strength occurs at 0.5% drift, and initial cracking occurs at 67% of peak strength at a drift ratio of 0.2%. The "a" and "b" versions of this spring differ in the slopes of the two strength-degrading segments, which are 5% and 13% (of the initial elastic stiffness) in Spring 5a, and 3% and 9% in Spring 5b. They also differ in the presence of a residual strength plateau, which exists in Spring 5a, but not in Spring 5b.

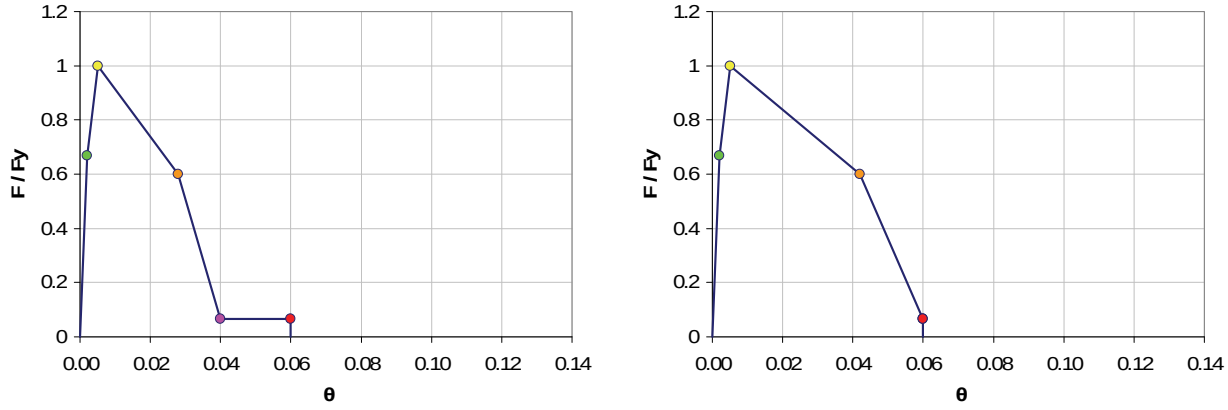

Figure 3-23 Force-displacement capacity boundaries for Spring 5a and Spring 5b.

The hysteretic behaviors of Spring 5a and Spring 5b, both with and without cyclic degradation, are shown in Figure 3-24 and Figure 3-25. They resemble a sliding system with cyclic degradation of strength, unloading, and reloading stiffness parameters. In each figure, the initial force-displacement capacity boundary (before cyclic degradation) is overlaid onto the hysteretic plots.

Systems with this type of behavior could include masonry walls and concrete frames with masonry infill. Results from experimental tests on these systems (Figure 3-26) exhibit a behavior that is similar to the behavior modeled in Springs 5a and 5b.

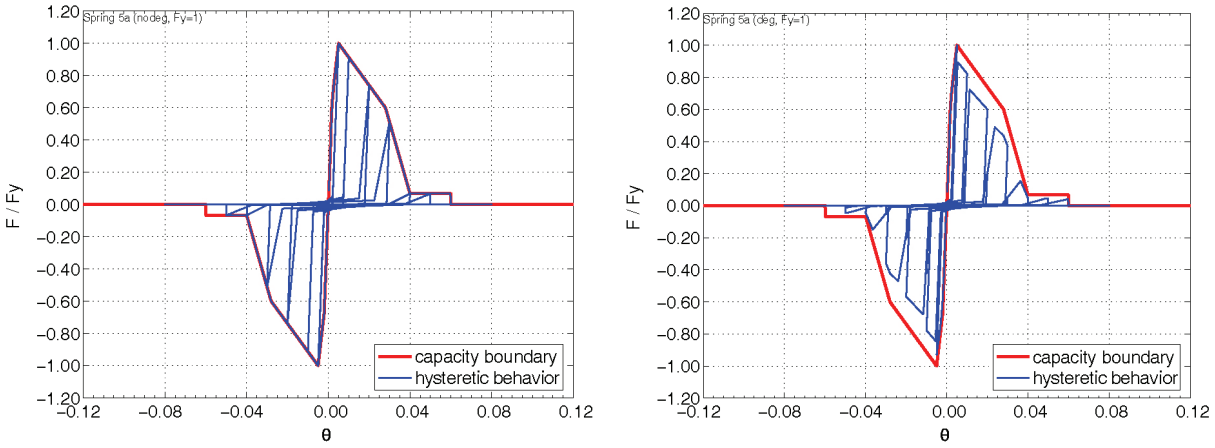

(a) (b)

Figure 3-24 Initial force-displacement capacity boundary overlaid onto hysteretic behaviors for Spring 5a: (a) without cyclic degradation; and (b) with cyclic degradation.

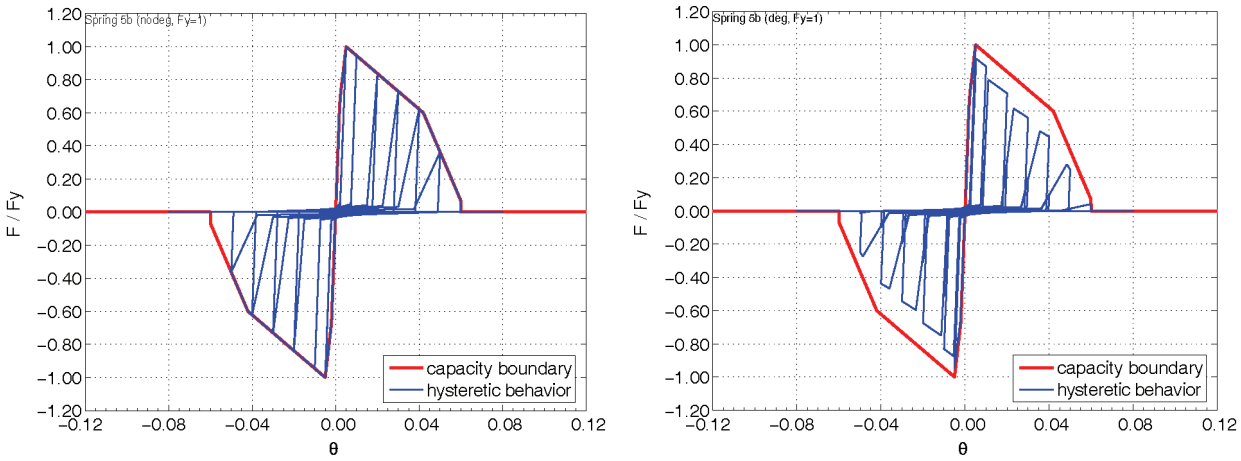

(a) (b)

Figure 3-25 Initial force-displacement capacity boundary overlaid onto hysteretic behaviors for Spring 5b: (a) without cyclic degradation; and (b) with cyclic degradation.

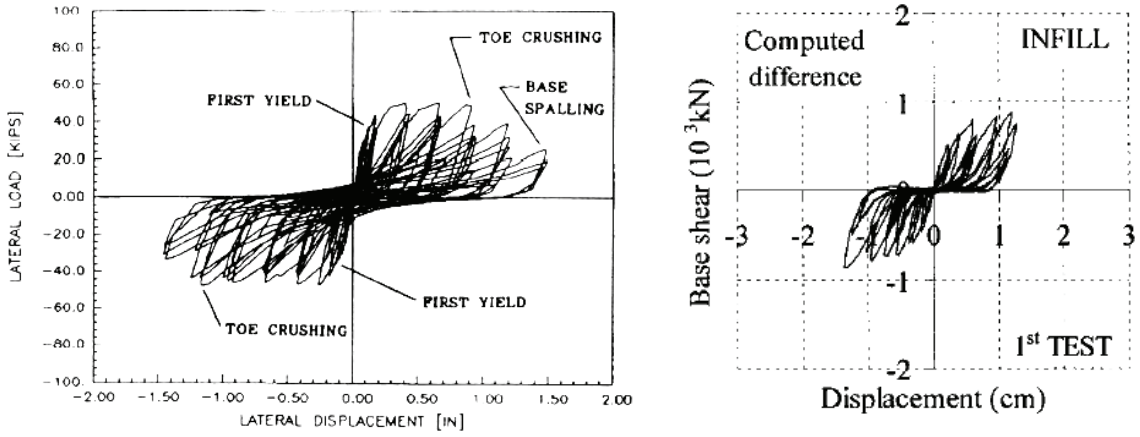

(a) (b)

Figure 3-26 Hysteretic behavior from experimental tests on: (a) reinforced masonry walls (Shing et al., 1991); and (b) concrete frames with masonry infill (Dolsek and Fajfar, 2005).

3.2.6 *Springs 6a and 6b – Elastic-Perfectly-Plastic Systems*

Springs 6a and 6b are intended to model the behavior of idealized elastic-perfectly-plastic systems with full, kinematic hysteresis loops, without any cyclic or in-cycle degradation of strength or stiffness. The force-displacement capacity boundaries are shown in Figure 3-27. The "a" and "b" versions of this spring differ in their finite ultimate deformation capacity, which is 7% drift in Spring 6a and 12% drift in Spring 6b.

Spring 6a and Spring 6b were analyzed with a constant force-displacement capacity boundary (no cyclic degradation). The resulting hysteretic behaviors are shown in Figure 3-28, with initial force-displacement capacity boundaries overlaid onto the hysteretic plots.

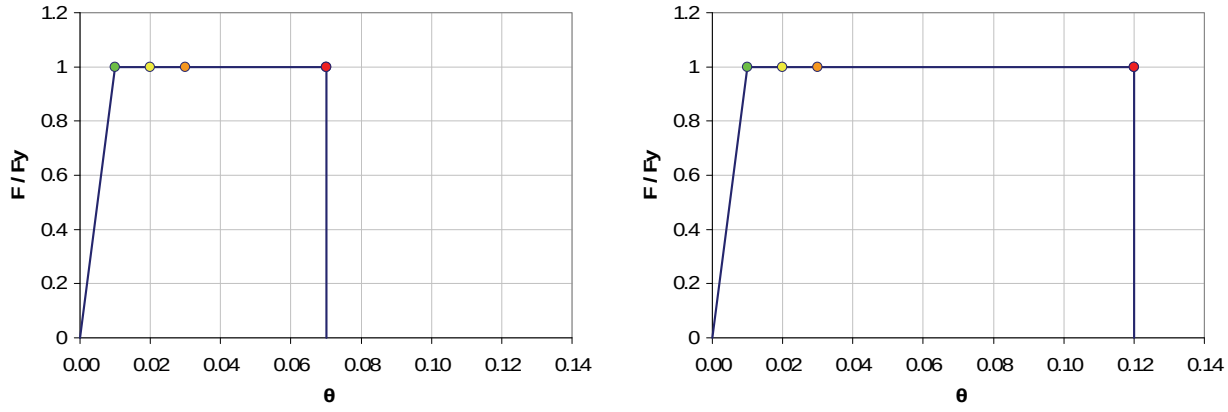

(Spring 6a) (Spring 6b)

Figure 3-27 Force-displacement capacity boundaries for Spring 6a and Spring 6b.

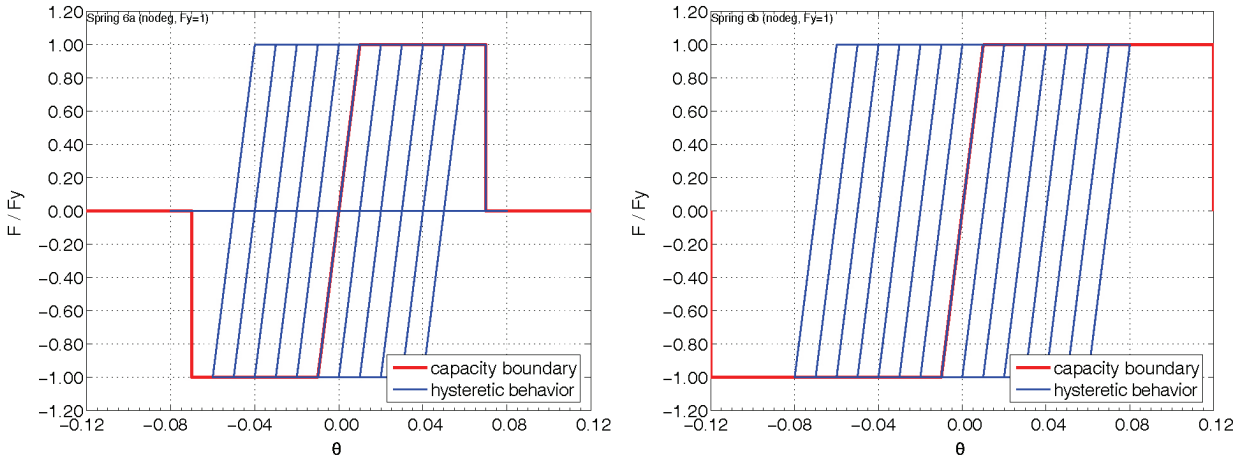

(a) (b)

Figure 3-28 Force-displacement capacity boundary overlaid onto hysteretic behaviors for: (a) Spring 6a without cyclic degradation; and (b) Spring 6b without cyclic degradation.

This is a highly idealized system developed for comparison of results. Practically speaking, only selected buckling-restrained braces or base-isolated systems would be capable of emulating this behavior under repeated cycles of large deformation demand.

3.2.7 *Springs 7a and 7b – Limited-Ductility Moment Frame Systems*

Springs 7a and 7b are intended to model the behavior of limited-ductility moment-resisting frame systems in buildings. They are characterized by a force-displacement capacity boundary with a short yielding plateau that maintains strength until a drift of 2%, followed strength degradation that terminates on a short residual strength plateau set at 20% of the yield strength (Figure 3-29). The "a" and "b" versions of this spring differ in the negative slope of the strength-degrading segment, which is negative 160% in Spring 7a and negative 40% in Spring 7b, and in the ultimate deformation capacity, which is 4% drift in Spring 7a and 6% drift in Spring 7b.

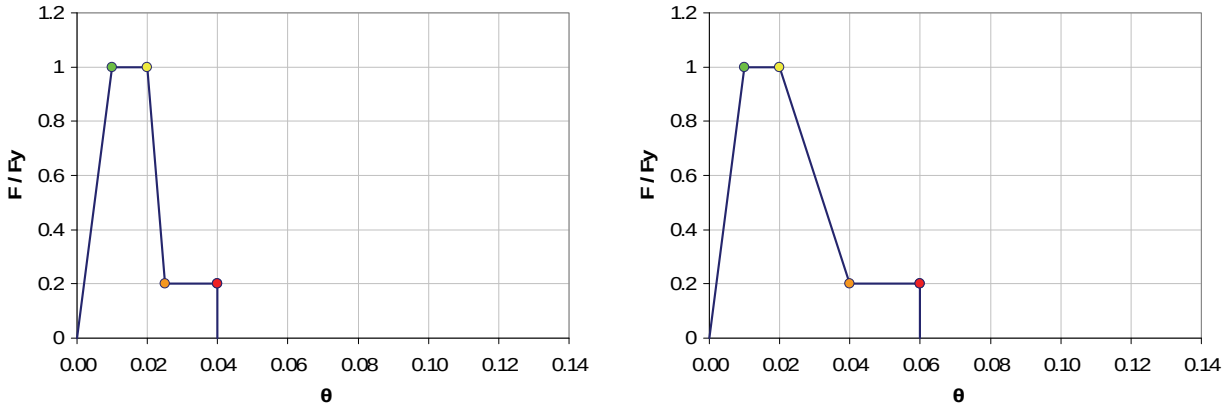

Figure 3-29 Force-displacement capacity boundaries for Spring 7a and Spring 7b.

The hysteretic behaviors of Spring 7a and Spring 7b, both with and without cyclic degradation, are shown in Figure 3-30 and Figure 3-31. In each figure, the initial force-displacement capacity boundary (before cyclic degradation) is overlaid onto the hysteretic plots.

Systems with this type of behavior could include older reinforced concrete frames not designed for seismic loads, which can be lightly reinforced, and may have inadequate joint reinforcement or concrete confinement. Results from experimental tests on lightly reinforced concrete columns (Figure 3-32) exhibit a behavior that is similar to the behavior modeled in Springs 7a and 7b.

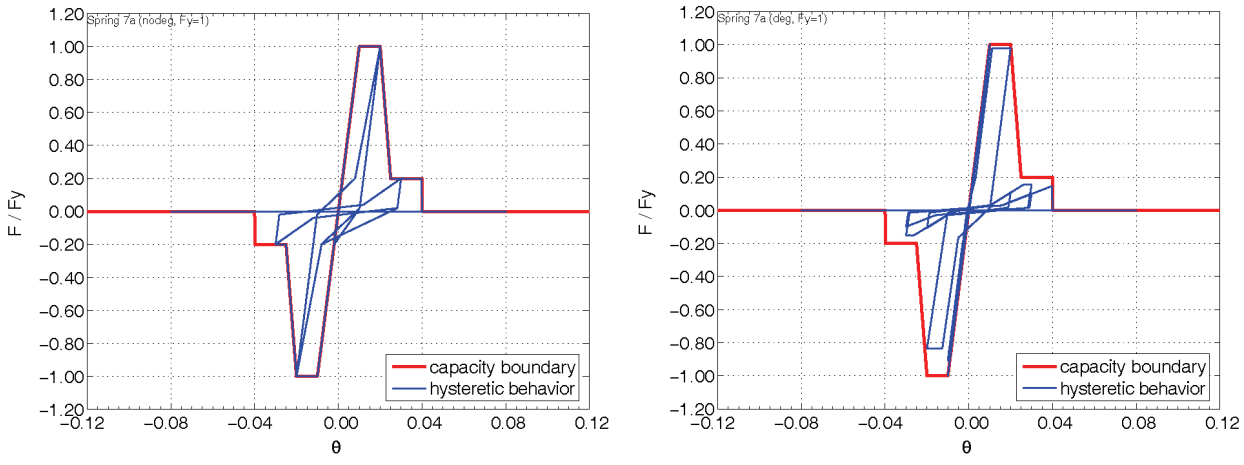

(a) (b)

Figure 3-30 Initial force-displacement capacity boundary overlaid onto hysteretic behaviors for Spring 7a: (a) without cyclic degradation; and (b) with cyclic degradation.

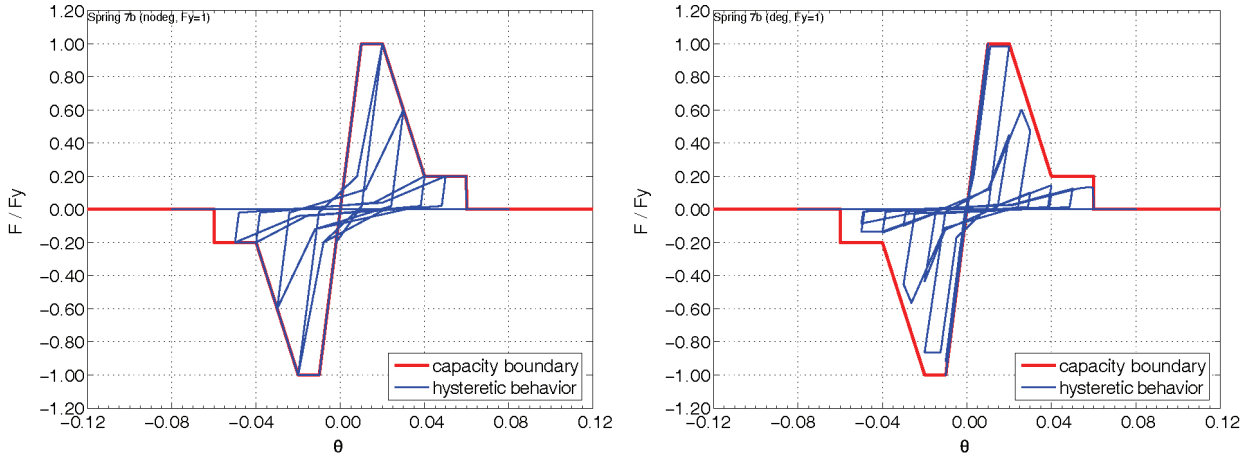

(a) (b)

Figure 3-31 Initial force-displacement capacity boundary overlaid onto hysteretic behaviors for Spring 7b: (a) without cyclic degradation; and (b) with cyclic degradation.

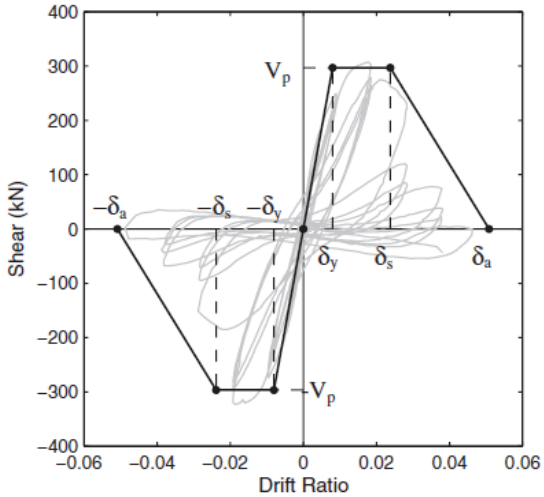

Figure 3-32 Hysteretic behavior from experimental tests on lightly reinforced concrete columns (Elwood and Moehle, 2006; Sezen, 2002).

3.2.8 *Springs 8a and 8b – Non-Ductile Gravity Frame Systems*

Springs 8a and 8b are intended to model the behavior of non-ductile gravity frame systems in buildings. The force-displacement capacity boundary includes significant strength degradation immediately after yielding, and limited ultimate deformation capacity (Figure 3-33). The "a" and "b" versions of this spring differ in the strength that is lost after yield, which is 100% in Spring 8a, and 45% in Spring 8b, and in the ultimate deformation capacity, which is 2.5% drift in Spring 8a and 4% drift in Spring 8b. They also differ in the presence of a residual strength plateau, which does not exist in Spring 8a, but does in Spring 8b.

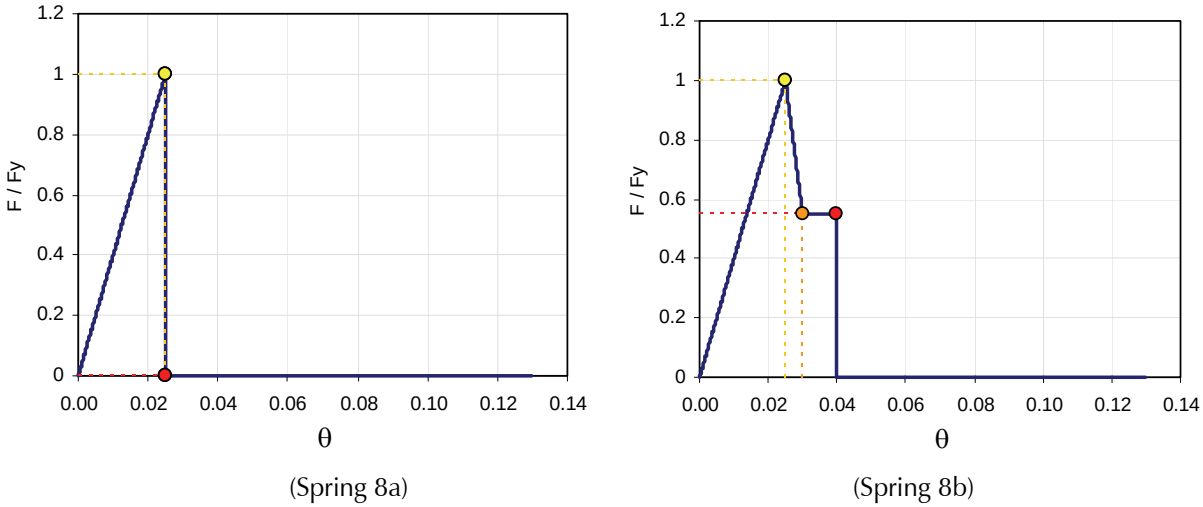

Figure 3-33 Force-displacement capacity boundaries for Spring 8a and Spring 8b.

The hysteretic behaviors of Spring 8a and Spring 8b, both with and without cyclic degradation, are shown in Figure 3-34 and Figure 3-35. In each figure, the initial force-displacement capacity boundary (before cyclic degradation) is overlaid onto the hysteretic plots.

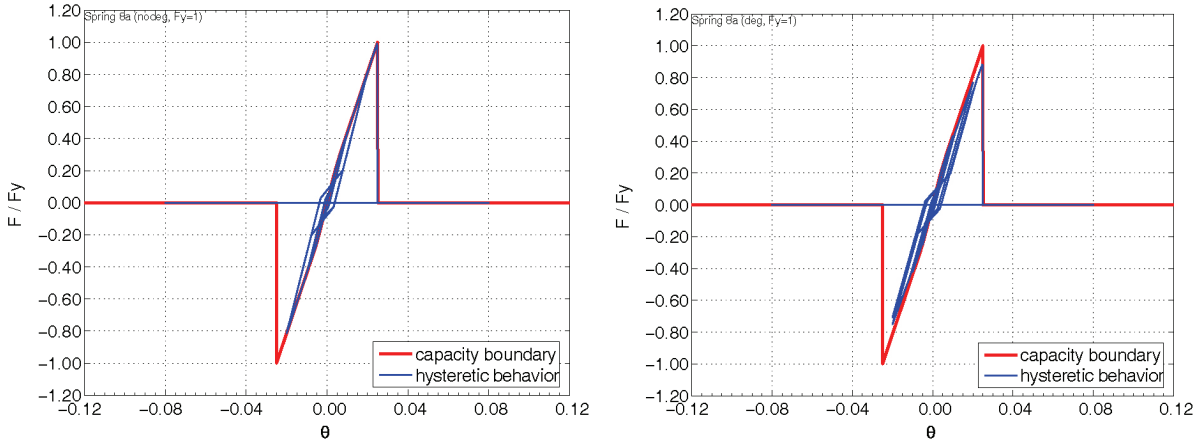

Figure 3-34 Initial force-displacement capacity boundary overlaid onto hysteretic behaviors for Spring 8a: (a) without cyclic degradation; and (b) with cyclic degradation.

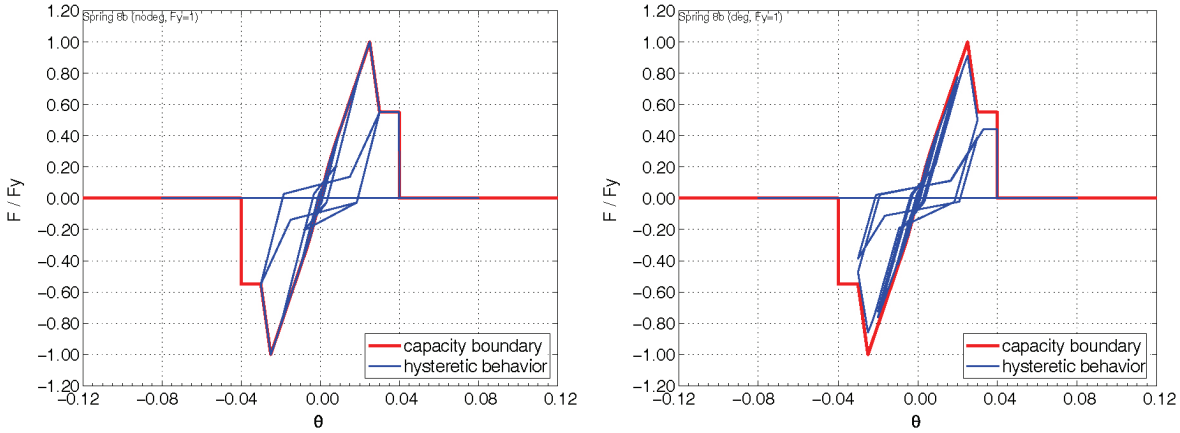

Figure 3-35 Initial force-displacement capacity boundary overlaid onto hysteretic behaviors for Spring 8b: (a) without cyclic degradation; and (b) with cyclic degradation.

3.3 Multiple Spring Models

Multiple spring models were used to represent the behavior of more complex structural systems containing subsystems with different hysteretic and force-displacement capacity boundary characteristics linked by rigid diaphragms. Multi-spring SDOF systems were developed by placing individual springs in parallel. Combinations were performed in a manner consistent with combinations that would be encountered in real structural systems. For each such combination, variations in the relative contribution of individual springs to the initial stiffness and maximum lateral strength over a range of periods were considered.

3.3.1 Multi-Spring Combinations of Single-Spring Systems

Of the numerous combinations possible, only assemblages consisting of two springs in parallel were considered in this investigation. Furthermore, only springs including cyclic degradation were considered in multi-spring combinations. This was done to limit the number of possible permutations under consideration, but also because, in general, realistic systems experiencing strong in-cycle degradation will also experience cyclic degradation.

Two-spring assemblages consisting of a lateral-force-resisting system (Springs 2, 3, 4, 5, 6, or 7), working in combination with a gravity frame system (Springs 1a, 1b, 8a, or 8b), were used. For example, a combination of Spring 2a with Spring 1a would be representative of a non-ductile moment frame system with a typical gravity frame back-up system in parallel.

In general, it is not realistic to assume that the contribution of each subsystem to the peak lateral strength of the combined system would be equal. In most cases, the lateral-force-resisting system in a building would be expected to be stronger and stiffer than the gravity system. For this reason, systems were combined using an additional parameter, N, as a multiplier on the contribution of lateral-force-resisting springs in the combined system. Multi-spring systems then carry a designation of "NxJa+1a" or "NxJa+1b" where "N" is the peak strength multiplier (N = 1, 2, 3, 5, or 9), "J" is the lateral-force-resisting spring number (J = 2, 3, 4, 5, 6, or 7), and 1a or 1b is the gravity system identifier. Using this designation, "3x2a+1a" would identify a system consisting of a multiple of three non-ductile moment frame springs (Spring 2a) in combination with a single gravity system spring (Spring 1a).

To investigate potential period-dependency, multi-spring systems were tuned to center the resulting periods of vibration for each set of "NxJa" lateral-force-resisting systems approximately around T=1.0s (representing relatively stiff systems) and T=2.0s (representing relatively flexible systems). This was accomplished by assuming two different story masses of M=8.87 tons or M=35.46 tons, respectively.

In summary the following series of multi-spring systems were investigated:

- Series 1: NxJa + 1a (M=8.87 ton; relatively stiff)
- Series 2: NxJb + 1a (M=35.46 ton; relatively flexible)
- Series 3: NxJa + 1b (M=8.87 ton; relatively stiff)
- Series 4: NxJb + 1b (M=35.46 ton; relatively flexible)

Multi-spring combinations using Spring 8a and Spring 8b were created and analyzed, however, the resulting behavior was not substantially different from other systems analyzed. As a result, this data was not investigated in detail, and information on these combinations has not been provided. As part of the series of investigations, each "NxJa" lateral-force-resisting system was analyzed without the 1a or 1b gravity system in order to compare results both with and without the contribution of the back-up system. A representative force-displacement capacity boundary from each multi-spring system is shown in Figure 3-36 through Figure 3-41.

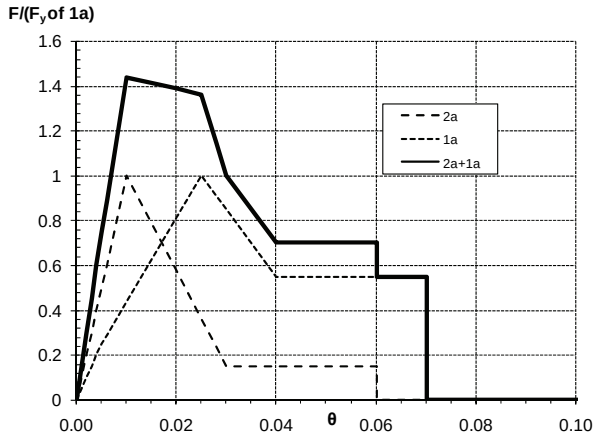

Figure 3-36 Combined force-displacement capacity boundary for spring 2a +1a (normalized by the strength of Spring 1a).

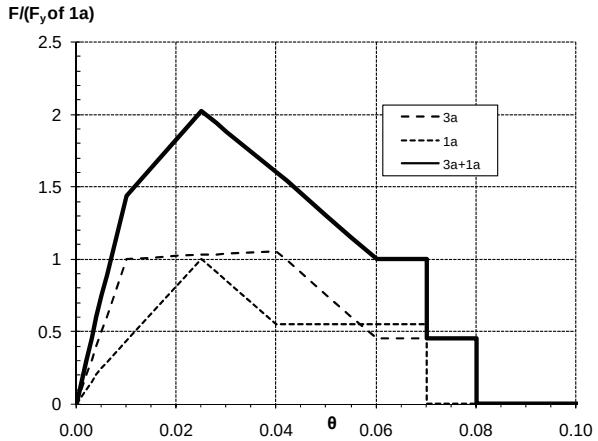

Figure 3-37 Combined force-displacement capacity boundary for spring 3a +1a (normalized by the strength of Spring 1a).

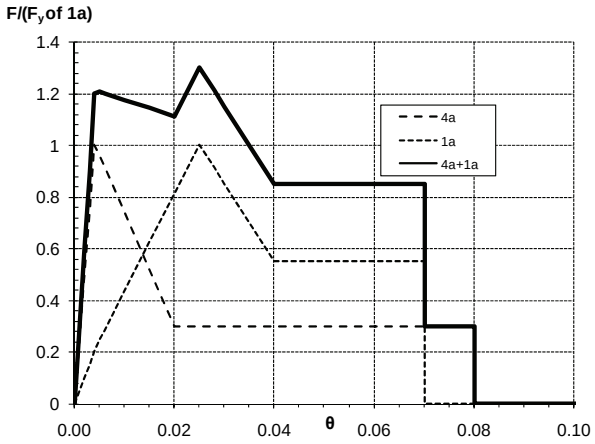

Figure 3-38 Combined force-displacement capacity boundary for spring 4a +1a (normalized by the strength of Spring 1a).

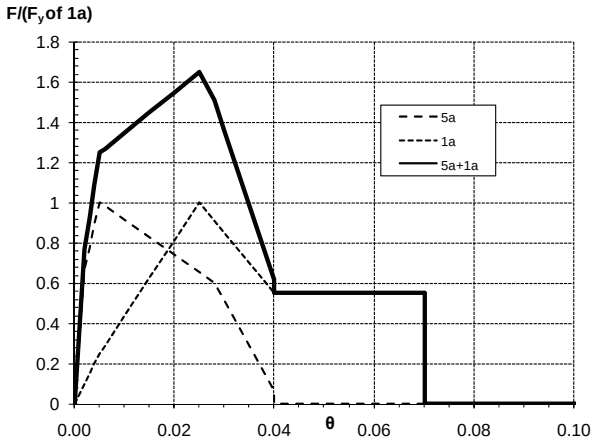

Figure 3-39 Combined force-displacement capacity boundary for spring 5a +1a (normalized by the strength of Spring 1a).

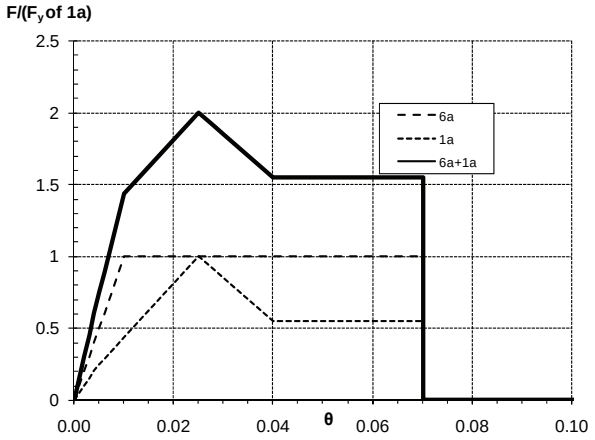

Figure 3-40 Combined force-displacement capacity boundary for spring 6a +1a (normalized by the strength of Spring 1a).

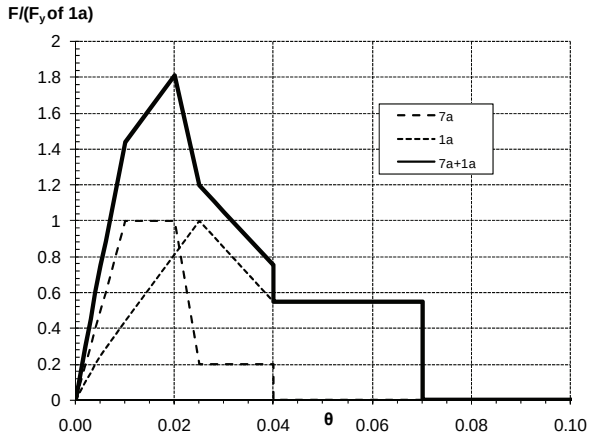

Figure 3-41 Combined force-displacement capacity boundary for spring 7a +1a (normalized by the strength of Spring 1a).

Each multi-spring combination was subjected to an ATC-24 type loading protocol with a degrading force-displacement capacity boundary (cyclic degradation). The resulting hysteretic behaviors for the combination of Nx2a+1a for (N = 1, 2, 3, 5, and 9) are shown in Figure 3-42 through Figure 3-44. In addition, individual Spring 2a is shown in Figure 3-44 for comparison. In each figure, the initial combined force-displacement capacity boundary (before cyclic degradation) is overlaid onto the hysteretic plots.

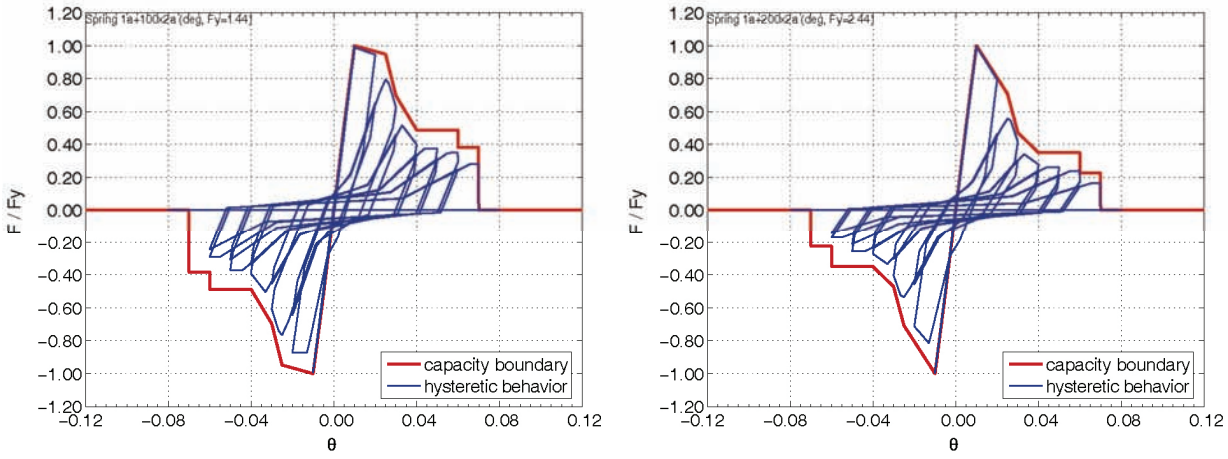

Figure 3-42 Initial force-displacement capacity boundary overlaid onto hysteretic behavior for: (a) Spring 1x2a+1a; and (b) Spring 2x2a+1a; both with cyclic degradation.

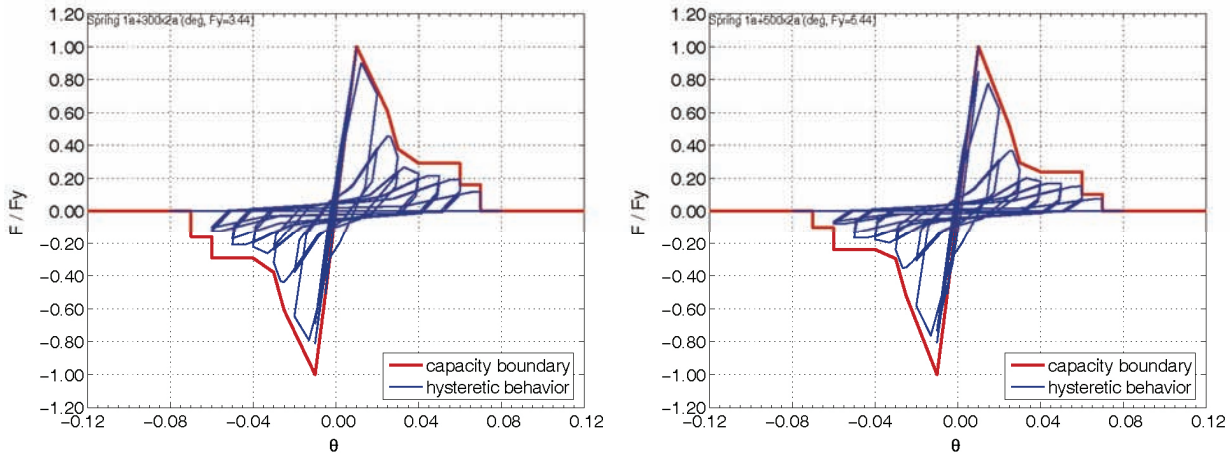

(a) (b)

Figure 3-43 Initial force-displacement capacity boundary overlaid onto hysteretic behavior for: (a) Spring 1x3a+1a; and (b) Spring 5x2a+1a; both with cyclic degradation.

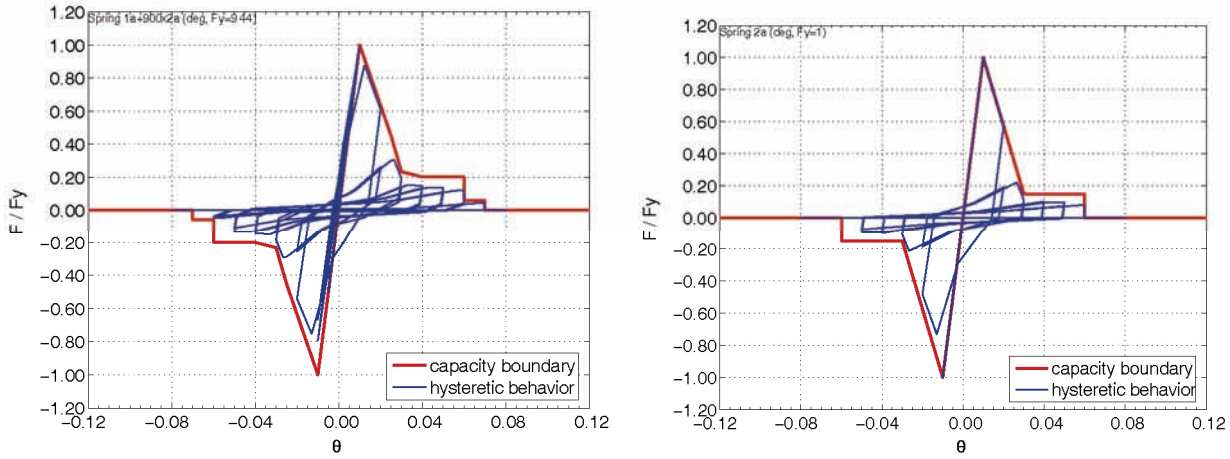

(a) (b)

Figure 3-44 Initial force-displacement capacity boundary overlaid onto hysteretic behavior for: (a) Spring 9x2a+1a; and (b) individual Spring 2a; both with cyclic degradation.

As might be expected, the more the multiplier "N" for Spring 2a increases, the more the combined system resembles Spring 2a itself (Figure 3-44), and the more the behavior of the combined system would be expected to be dominated by the characteristics of the lateral-force-resisting spring component. Conversely, for lower multiples of "N", the characteristics of the gravity system are more visible in the combined system properties (Figure 3-42), and would be expected to play a more significant role in the behavior of the combined system.